RARE METALS

Understanding and modifications on lithium deposition in lithium metal batteries

Qin-Ya Yang, Zhao Yu, Yao Li* , **Wang Zhang, Hao-Wen Yuan,**
Hong-Jie Li, Wei Ma, Shen-Min Zhu, Sa Li*

Abstract Lithium metal has been considered as an ultimate anode choice for next-generation secondary batteries due to its low density, superhigh theoretical specific capacity and the lowest voltage potential. Nevertheless, uncontrollable dendrite growth and consequently large volume change during stripping/plating cycles can cause unsatisfied operation efficiency and serious safety concern, restraining its commercial use for the last 40 years. As widely used lithium-ion battery is approaching its theoretical limit at present, it is increasingly urgent to develop new energy storage equipment with sufficient practical capacity. Herein, two important processes of lithium deposition, nucleation and growth on lithium metal anode are reviewed. Modified three-dimensional (3D) porous anodes with unique structure and dynamic surface conditions, as one of the most efficient designs on dendrites suppression, are specifically discussed in terms of their beneficial adjustment on the dendrite formation. Problems on current designs and prospects on future advanced porous anode are explored in the end.

Keywords Lithium metal batteries; Lithium nucleation; Dendrites growth; Porous anodes

Q.-Y. Yang, Z. Yu, Y. Li*, W. Zhang, H.-W. Yuan, H.-J. Li,
W. Ma, S.-M. Zhu
State Key Laboratory of Metal Matrix Composites, School of
Materials Science and Engineering, Shanghai Jiao Tong
University, Shanghai 200240, China
e-mail: liyaosjtu@sjtu.edu.cn

S. Li*
School of Materials Science and Engineering, Tongji University,
Shanghai 201804, China
e-mail: lisa@tongji.edu.cn

1 Introduction

The rapid development of modernization and industrialization causes wide concerns in human society about energy storage and environmental problems [1, 2]. Lithium-ion battery (LIB) is an outstanding example of an energy storage device. Charge storage and charge transfer in LIBs are achieved by Li^+ intercalation and deintercalation of carbon or compound lattice in the cathodes [3, 4] (Fig. 1a). Commercial lithium-ion batteries can have a long-lasting operation over 1000 cycles steadily without safety problems [5]. Relatively light, durable and environmentally friendly LIBs compared to traditional lead-acid batteries have largely promoted the development of portable electronic devices and modern electric vehicles, as approved by 2019 Noble Prize in Chemistry awarded to three scientists who have made great contributions to the research and industrialization of lithium-ion batteries [6, 7].

However, even the best commercial LIB cannot meet the high energy density required for advanced power vehicles, as the theoretical limit of graphite anode is only 376 mAh·g^{-1} [8]. Novel cathodes/anode materials are urgently needed. Lithium metal is believed to be a promising candidate for advanced high-energy-density anodes [9]. Due to the lowest electrochemical potential of lithium metal (–3.04 V versus standard hydrogen electrode), lithium metal battery can obtain high voltage difference in full cell configuration, allowing abundant charge release before the end of the discharge process [10]. Moreover, the density of lithium metal is only 0.534 g·cm^{-3}. During discharge, one lithium atom dissolves into an electrolyte accompanied by one-electron transfer. According to Eq. (1), the specific capacity of lithium metal anode is 3860 mAh·g^{-1} [11]:
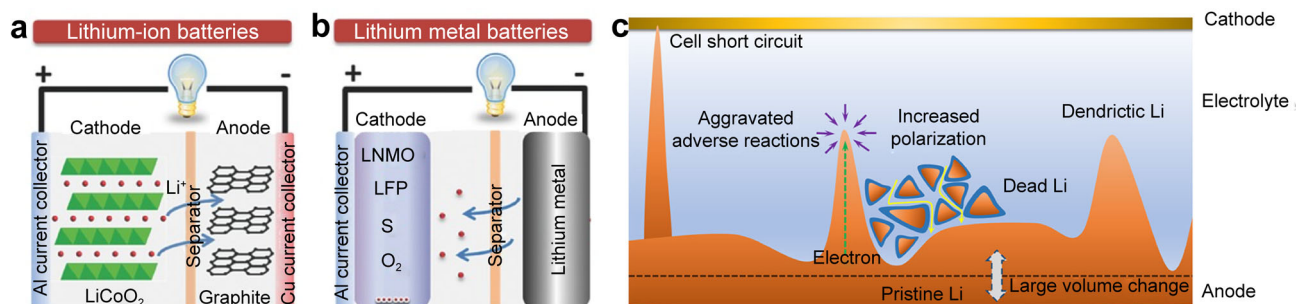
Fig. 1 Schematic comparison between **a** lithium-ion battery and **b** lithium metal battery. Reproduced with permission from Ref. [4]. Copyright 2017, WILEY–VCH. **c** Schematic illustrations of possible problems in lithium metal battery during operation. Reproduced with permission from Ref. [10]. Copyright 2017, American Chemical Society

$$C_0 = \frac{F \cdot n}{3.6 \cdot m} \approx 26801 \frac{n}{m} \tag{1}$$

where F is Faraday constant (96,485 C·mol^{-1}), n is the number of charges per mole reaction, m is the mass of anode materials per mole, C_0 is the specific capacity of materials. The ultra-high-energy-density lithium metal battery (2600 Wh·kg^{-1} for Li–S battery, 3505 Wh·kg^{-1} for Li–O$_2$ battery) is regarded as the most potential energy storage device for next-generation electric vehicles [4, 12] (Fig. 1b). Nevertheless, disadvantages of lithium metal battery are also prominent. Li metal with body-center-cubic (bcc) structure has large adsorption energy (–1.13 eV at bridge site on (001) surface). Interaction between Li adatoms is also weak [13]. As a result, deposited Li atoms prefer to stay isolated rather than aggregate to form stable nucleation sites. Surface energy of lithium metal is also low (0.46 J·m^{-2} for (100) surface), leading to dendritic lithium deposition with a large surface area [14].

Uncontrollable lithium dendrite is the most serious problem for lithium metal anode (Fig. 1c). Firstly, alkali lithium metal has very high chemical activity. The Fermi energy of lithium atoms is higher than the lowest unoccupied molecular orbital (LUMO) of most polar solvents and lithium salt additive anions [15]. Therefore, lithium metal is easy to react with electrolytes to form a solid electrolyte interphase (SEI) [16]. Large surface area of fractal lithium dendrites increases the contact area between lithium metal and electrolyte, resulting in large consumption of active lithium and electrolyte [17]. What's more, naturally formed solid layer at the interphase between lithium metal and electrolyte is heterogeneous and brittle. Dendritic lithium, on the contrary, has a high yield strength [18]. Protrusion of SEI layer exposes fresh lithium metal to the organic electrolyte, aggravating the adverse reactions which accelerate the depletion of active reactants in the battery and capacity decay [19]. Secondly, relatively weak roots of lithium dendrites may fracture and lose electron contact from base metal, because of the electron insulating

SEI layer covering the broken sites [20]. These "free" lithium dendrites, named as "dead" lithium neither participate in electrochemical reaction nor contribute to battery capacity [21]. Loose "dead" lithium spreading around the anode hinders the ion transportation, increases polarization and interphase impedance, leading to extra voltage loss. Lastly, large volume change coming from continuous dendrite growth and partial dissolution exacerbates the instability of anode structure and charge/discharge performance [22]. Tip-growth threadlike lithium dendrites can penetrate separator and reach the cathode. Short circuit consequently occurs, causing battery failure even explosion [23, 24].

Dangerous lithium dendrite is the biggest barrier to the practical application of lithium metal battery. Although the original design of lithium battery was based on lithium metal anode, scientists had to change the road to a safer system, which is lithium-ion battery, in order to take advantage of light and small radius lithium. Nevertheless, current lithium-ion battery has almost reached its theoretical capacity limit. Higher energy density storage equipment is urgently required for the further development of electric devices [25]. In the past 20 years, deposition/dissolution behavior of lithium metal anode and its impact on the full cell are gradually revealed. Strategies on restraining lithium dendrites and stabilizing battery performance are also reported to be effective in the laboratory [26]. Although current understanding and corresponding designs of lithium metal battery are difficult to meet the requirement of industrialization and commercialization, possible approaches toward advanced lithium metal battery are becoming clear. Several recognized principles have been established and developed continuously [27].

In this review, lithium deposition behaviors in lithium metal battery including nucleation, dendrite growth and their co-effect are summarized. Corresponding principles on regulating these two processes are also reviewed. Modified three-dimensional (3D) porous anodes, as an

important method on regulating both lithium nucleation and dendrite growth, is specifically discussed. Finally, problems of existing current designs and the prospect of future development of advanced 3D porous anode are presented.

2 Fundamental of lithium dendrites and modifications on lithium deposition

2.1 Nucleation

Driven by electric field of double electric layer, a Li^+ moves to anode, gets an electron and deposits on the surface. At the same time, Li atoms at the stage of thermodynamic instability lose electrons and redissolve into electrolyte. When the deposited lithium aggregates to a critical nuclei size, these Li clusters are able to exist stably and grow continuously [28, 29]. Defects of anodes such as dislocations, grain boundary cracks with high electrons concentration and large electric field are preferable to Li deposition. Highly conductive solid ceramic electrolytes and inner pores with excess electrons or negative charges also facilitate Li^+ reduction [30, 31]. Li nucleation may also occur inside bulk lithium metal anode due to the inner contaminants such as Li_3N in solid polymer electrolyte system [32]. Further deposition is prior to existing nuclei, leading to heterogeneous nucleation [33]. Li deposition inside solid electrolytes is dangerous because it renders the possibility of fast short circuits in lithium metal battery. Extremely low conductivity of solid electrolytes helps restrain inner dendrites formation [34]. Tiny and homogeneous nucleation on the anodes is desirable in terms of stable battery operation. Based on the heterogeneous nucleation model, smooth anode surface is required for homogeneous nucleation while fabrication of a perfect surface without any defects in large scale is almost impossible. Pre-distributing chemical active sites or "nucleation seeds" on the anode is an alternative method to guide lithium deposition [35]. "Nucleation seeds" decrease lithium nucleation overpotential by increasing wettability between current collector and lithium metal [36]. Successful examples include organic ligands, such as –NH [37] and –OH [38], which provide extra electrostatic interaction. Metals, including Au [39] and Ag [40], can form alloys with lithium at room temperature and oxides such as Co_3O_4 [41], ZnO [42] showing high reaction wettability with Li are also used as active seeds to uniform Li deposition. As-formed alloys not only have higher surface energy and electrochemical stability than that of pure lithium metal, but also remain lithiophilic nature to guide further electrodeposition through alloying-dealloying

process, resulting in less formation of subsequent lithium dendrites and side reactions [43].

2.2 Dendrite growth

After a nucleus stably exists, Li^+ in the electrolyte driven by current density can continuously deposit on the substrate, resulting in nucleus growth. High deposition rate causes the depletion of Li^+ near the nuclei. Huge space-charge electric field forces the rapid Li deposition towards the reverse direction of the largest concentration gradient, leading to uncontrollable dendrites [44]. The critical time when ion concentration in the anode-electrolyte interphase decreases to zero is named as "Sand's time". "Sand's time" represents the dividing line between smooth plating and fractal lithium dendrites. It was firstly reported by Sand [45] in 1901 for describing electrodeposition behavior of copper ion in binary electrolyte, when copper salt concentration decreases to zero near the cathode after which hydrogen occurs at constant current density. In the lithium metal battery system, Sand's time could be measured by voltage–time profile and defined as the time when the second spike appears (Fig. 2a, b). "Experimental Sand's time" can be defined by real-time optical observation as the time when the first dendrite appears (Fig. 2c) [46]. Equation (2) gives the mathematics description of Sand's time (t_{Sand}):

$$t_{Sand} = \pi D_{app} \frac{(Z_c C_0 F)^2}{4(J t_a)^2} \tag{2}$$

where D_{app} is the diffusion coefficient, Z_c is the charge number of electroplating cations, C_0 is the salt concentration, F is the Faraday constant (96,485 $C \cdot mol^{-1}$), J is the current density, t_a is the transference numbers of the discharging anions. According to Eq. (2), low current density, high ion concentration and transference number delay the time for dendrites growth.

2.2.1 Current density

Current density is defined as the amount of charge per unit time passing through a unit area. It represents the redox reaction rate on anode/electrolyte interphase. Violent reduction reaction accelerates ion depletion near the surface of anode during charge cycle. Bai et al. [47] defined two characteristic current densities J_{cc} and J_{lim} based on morphology change in liquid electrolyte system to divide the whole plating process into three parts (Fig. 2d): $J < J_{cc}$ for root-growing whiskers, $J_{cc} < J < J_{lim}$ for prevailing surface growth and $J > J_{lim}$ for tip-growing dendrites. Relatively large current density ($J > J_{cc}$) will more likely result in the penetration of lithium dendrites into separators
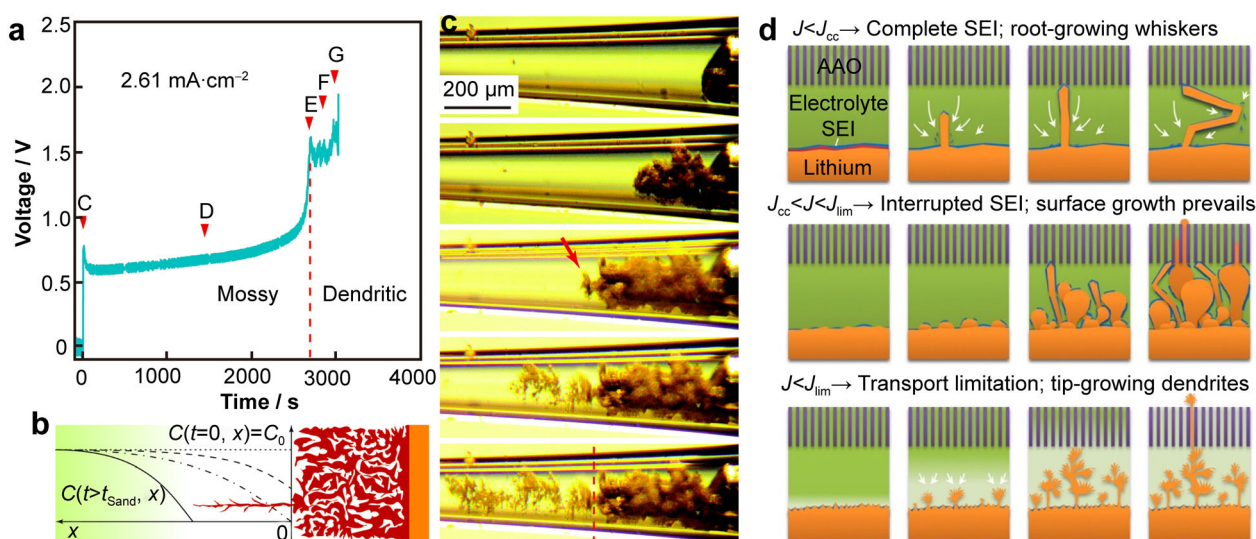
Fig. 2 Sand's time theory and corresponding morphology evolution. **a** Voltage–time profile of discharging cycle at current density of 2.61 mA·cm^{-2}; **b** schematic illustration of lithium dendrite at Sand's time pointed in **a**; **c** real-time optical observation of dendrite growth, where red arrow points to primary lithium dendrite, red dash line shows boundary between mossy whiskers and fractal dendrites. Reproduced with permission from Ref. [46]. Copyright 2017, The Royal Society of Chemistry. **d** Morphology evolution of lithium deposition under different current densities. Reproduced with permission from Ref. [47]. Copyright 2018, Elsevier B.V

and cause battery failure. Surface morphology on lithium metal anode changes from root-growing on the base metal to rapid tip-growing serpentine dendrites during plating half-cycle. It is worth mentioning that Joule heat generated by ultra-large current density on metal anode may also melt the dendritic structure of deposited lithium, thus stabilizing charge–discharge cycling [48].

2.2.2 Ion distribution

Uniform and stable Li$^+$ distribution in the deposition area are ideal for homogeneous lithium plating and long duration time of lithium metal battery, especially cycling at a high rate. Direction and velocity of moving Li$^+$ can be affected by electric field in the battery, subsequently influencing the ion distribution and dendrites growth. Chazalviel et al. reported that the velocity of dendrites tips was reversely proportional to the electric field strength based on a thin rectangular cell model [44]. Although this model did not take the diffusion factor into account, it still revealed the effect of the electric field, especially during the early stage in the charging process. Zou et al. [49] pointed out that homogeneous electric field distribution was vital to uniform electrodeposition while local aggregated electric field at defect or dendrites' tips facilitated heterogenous ion distribution and accelerated unstable plating process.

Besides electric field, ion distribution is largely affected by ion concentration and ion movability in the lithium metal battery. According to Sand's time theory, large salt concentration ensures a steady and sufficient ion supply for the reduction reaction, as well as to delay and restrain electrolyte depletion [50]. However, the high viscosity and poor wettability of concentrated liquid electrolytes can harm the operational performance of lithium metal batteries [51, 52]. Utilizing the synergistic effect of different electrolytes can help solve this dilemma [53]. Besides enhancing ion-concentration in the whole electrolyte, narrowing or even eliminating zero-concentration region near deposited Li clusters is also effective to suppress lithium dendrites [54]. For example, the Lorentz force caused by the magnetic flux around the dendrite tip can guide Li$^+$ away to achieve uniform lithium deposition [55]. High ion conductivity can also replenish cations quickly and maintain ion concentration at thermodynamic equilibrium, thereby affecting dendrites formation [56, 57].

Li$^+$ in the electrolyte needs to go through SEI layer before electroplating [58]. Therefore, the high Li$^+$ conductivity in SEI layer plays a decisive role in ion concentration. SEI layer results from side reaction between active Li, ambient atmosphere and electrolyte [16]. It is composed of inner inorganic components such as Li$_2$O, LiF, LiCO$_3$, and outer organic components such as LiCOOH, RCOO$_2$Li [59]. SEI layer is electron insulating but ion conductive. Highly ion-conductive SEI layer can help maintain homogeneous ion-concentration on anode side, leading to uniform lithium deposition [60]. It has been reported that ratio of dendritic to spherical lithium deposition decreases with decreased current density and increased ion-conductivity of SEI layer [61]. SEI layer riches in LiF has high

Li^+ conductivity with energy barrier (E_b) of only 0.19 eV in a vacuum and large surface energy with high stability. Electrolyte solvents such as fluoroethylene carbonate (FEC) [62], fluorosulfonamide (FSA) [63], N,N-dimethyl-trifluoromethane-sulfonamide (DMTMSA) [64] and salts in electrolytes such as lithium bis(fluorosulfonyl)imide (LiFSI) [65], lithium bis(trifluoromethanesulfonyl)imide (LiTFSI) [66] are proved to be beneficial in the formation of LiF-riched inorganic SEI layer. A thin LiF layer for stabilizing lithium deposition can also be obtained by pre-treatment of anodes before cell assembly. For example, Yuan et al. [67] dropped NH_2HF_2 on the surface of lithium metal to fabricate a thin and porous LiF layer (Fig. 3a). This artificial LiF layer promotes flat lithium deposition by lowering the activation energy for dendrite growth towards lateral direction. Full cell with LFP cathode had a CE over 99% at 340 $mA \cdot g^{-1}$ over 100 cycles.

The components and additives of liquid electrolyte will affect the stability of SEI layer, and then affect the ion conduction rate in SEI layer. Electrolyte additives such as $LiNO_3$ [68], Mg^{2+} [69], Ga^{2+} [70] are usually used for modifying lithium plating through in-situ reactions on the metal anode to stabilize the SEI layer. However, these additives are gradually consumed as SEI layer reforms continuously in cycling, so that their functionality to suppress Li dendrite growth deteriorates inevitably. One novel way to supply additives is to assemble the additional components within the metal anode. It has been recognized that $LiNO_3$ and lithium metal powder (LMP) can be mixed to prepare $LiNO_3$ pre-planted lithium metal powder anode [71]. $LiNO_3$ powder partly reacts with fresh metal on the surface of LMP to form a N-enriched protective mask, resulting in dense and spherical lithium deposition (Fig. 3b). Residual $LiNO_3$ is stored inside intervals between lithium particles. These extra $LiNO_3$ powders generally dissolve into the electrolyte and supply the additives consumption in prolonged cycling. Moreover, direct addition of $LiNO_3$ into carbonate-based electrolyte
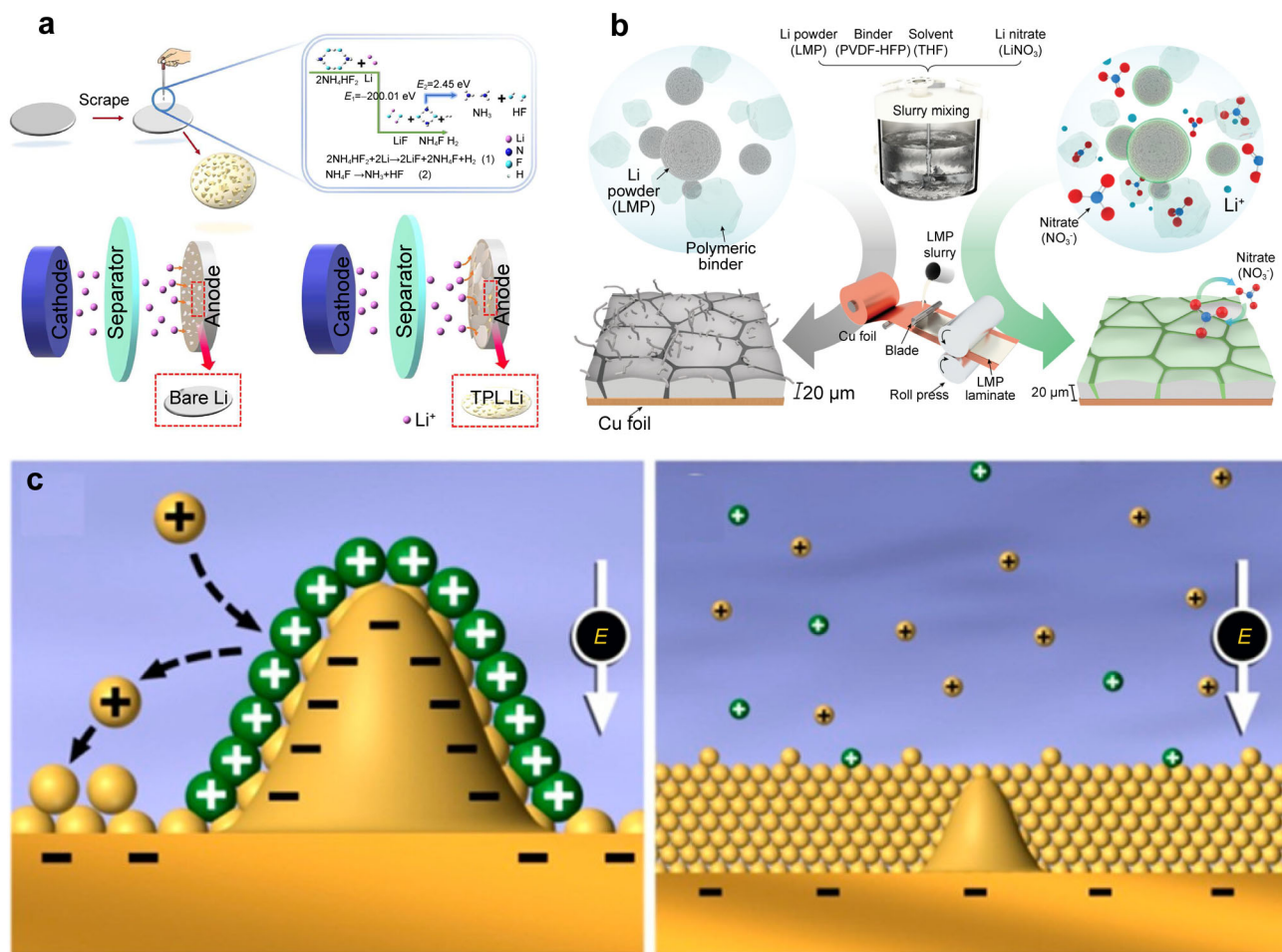

Fig. 3 Regulating ion distribution for stable lithium deposition. **a** LiF-rich addition on SEI layer for fast ion conductivity. Reproduced with permission from Ref. [67]. Copyright 2019, Elsevier B.V. **b** $LiNO_3$-LMP composited anode for extending life of robust SEI layer. Reproduced with permission from Ref. [71]. Copyright 2021, WILEY–VCH. **c** Adjustment of ion distribution based on SHES mechanism. Reproduced with permission from Ref. [73]. Copyright 2013, American Chemical Society

may restrain other additives like PF_6^- to make effect on constructing robust SEI layer because of the earlier reduction process of $LiNO_3$ than PF_6^-. However, $LiNO_3$ inside LMP composite anode does not participate in the initial decomposition of electrolyte. Therefore, effective components like LiF can successfully form and even be intensified under the effect of $LiNO_3$. Full cells of 20 μm $LiNO_3$-LMP composite anode and NMC622 with negative/positive electrode capacity (N/P) ratio of only 1.1 steadily operated 120 cycles at 1/3C with over 96% capacity retention. Another way to keep additives concentration is to change their working mechanism from modifying SEI layer to control electrochemical reaction conditions. This category of additives includes Cs^+ and Rb^+ based on self-healing electrostatic shield (SHES) mechanism [72]. Take Cs^+ for example, Cs^+ has a larger reduction potential (–2.925 V) than Li^+ (–3.04 V) under standard measurement when cation concentration is 1 mol·L^{-1}. However, reduction potential of Cs^+ can be lower than that of Li^+ when their concentrations are less than 0.1 mol·L^{-1} according to Nernst equation. When applying a potential higher than $E_{Cs/Cs+}$ but lower than $E_{Li/Li+}$, small bump on the surface from Li^+ reduction has higher negative charge density attracting both Cs^+ and Li^+ to its tip. Under the effects of charge repulsion and electrostatic shield, Li^+ is repelled from small dendrites to vicinity and achieve homogeneous distribution (Fig. 3c). In contrast, Cs^+ is functioned as a leveling agent with no consumption [73]. Nevertheless, the SHES mechanism only works on elements with similar deposition potential as lithium, so the applied potential needs to be precisely controlled to avoid co-deposition of Li^+ and additive cations.

Realization of uniform ion distribution in solid-state electrolyte (SSE) is critical because Li^+ movability in SSEs by solid diffusion is much harder than that in liquid electrolytes. Slow ion compensation rate in SSEs limits the application of solid-state batteries at high current density and rate cycling [74]. Large concentration difference at anode-electrolyte interphase promotes the establishment of a double-layer electric field and accelerates dendrites formation. Inorganic solid electrolytes usually have faster Li^+ movability (1×10^{-4}–1×10^{-2} $S·cm^{-1}$) than polymer electrolytes (1×10^{-8}–1×10^{-5} $S·cm^{-1}$) [75]. Solid-state electrolytes with sulfide have relatively high ion conductivity. For example, argyrodite-type solid-state electrolyte can achieve ionic conductivity of 1 $mS·cm^{-1}$ [76]. Addition of active fillers with intrinsic high Li^+ conductivity or passive fillers for the introduction of glassy region in polymer electrolyte can accelerate Li^+ movability in SSEs [77, 78]. Aligning fillers to construct straight and continuous Li^+ channels in SSEs is also effective to increase ion conductivity and rate performance of SSEs [79]. Since most high ion-conductive SSEs were tested at temperatures over 40 °C, desirable ion distribution at room temperature remains challenge for the further development of solid-state lithium metal batteries.

2.2.3 Force

Tips of lithium dendrites can produce stress as high as 130 MPa. Lithium whiskers also show a yield strength of 244 MPa under pure stress load according to in-situ measurements in atomic force microscope [18]. The mechanical strength of SEI layer will have a certain impact on the growth of lithium dendrites. Naturally formed SEI layer is usually brittle and hard to withstand such high mechanical stress. Broken SEI losses its effect on blocking electrolyte from contacting fresh metal, leading to further side reaction and capacity loss [80]. Thin but strong SEI layer is ideal because of less consumption of Li^+ and large surface tension induced by high elastic module [81]. Artificial SEI layer such as carbon-based materials and modified glass fiber are believed to make sense due to their good conductivity and high mechanical strength [82]. As a typical example, Zheng et al. [83] fabricated interconnected hollow carbon nanospheres on the surface of lithium metal anode using a template synthesis method. The carbon layer had a Young's modulus around 200 GPa which was sufficient to prevent dendrites growing. Results showed that the dendrites beneath hollow carbon nanospheres were thick and coarse. In addition, carbon-spheres thin film was loosely attached to the current collector and it could move freely to accommodate volume change during Li plating.

Besides SEI layer, extra strength from physical pressure outside battery, separator and solid electrolyte are also reported effective in dendrites suppression [84]. Applying stress on dendrites can induce horizontal deposition direction. Short and thick lithium dendrites with dense morphology can be achieved under physical pressure [85]. Coarse dendrites with a low specific surface area have low electrolyte consumption, thereby extending the lifespan of lithium metal battery. External mechanical force on lithium metal battery is achievable on flat pouch cells or coin cells [86]. However, it is hard to apply in cylindrical cells and large devices in practice. To solve this problem, researchers introduce stress constraints inside the battery such as nanoporous ceramic separators, which can efficiently prevent dendrites penetration [87]. Reducing the pore size can further suppress dendrite penetration but may impede normal ionic flow [88]. Recently, scientists conducted surface modification on separators to improve the wettability of electrolytes and methods to restrain dendrites penetration [89]. For example, a nano-shielded (NS) separator whose curved surface is composed of SiO_2 nanoparticles takes advantage of this idea [90] (Fig. 4a).
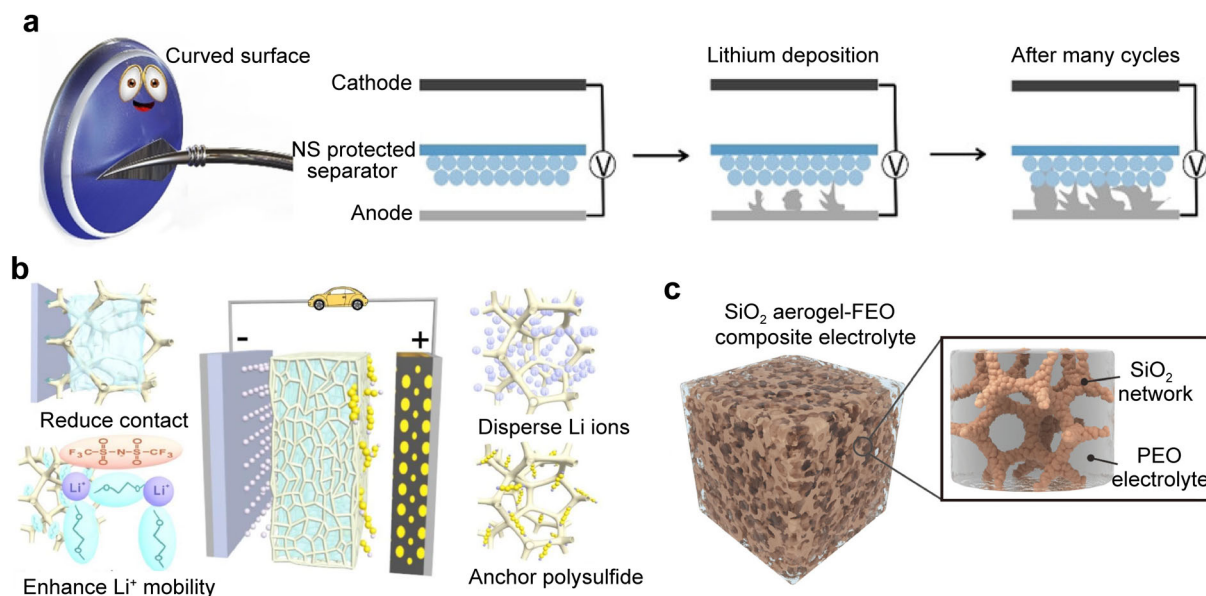
Fig. 4 Introducing force in LMBs for lithium suppression. **a** Controllable force from curved nano-shield (NS) separator. Reproduced with permission from Ref. [90]. Copyright 2020, WILEY–VCH. **b** Adding force from carbonized melamine sponge (HCS) separator. Reproduced with permission from Ref. [91]. Copyright 2021, Elsevier B.V. **c** Applying physical pressure from solid state electrolyte (SSE). Reproduced with permission from Ref. [100]. Copyright 2018, WILEY–VCH

Curved shield deflects the tip growing direction and reduces the equivalent stress to the separator. Limited space between nanoparticles can also help to prevent the penetration of lithium dendrites. Xu et al. [91] took use of carbonized melamine sponge (HCS) as a separator for stable lithium metal battery (Fig. 4b). Rich –N and –COOH ligands on carbon foam regulated the interaction between Li^+ and solvent molecules. Mobility of Li^+ in the electrolyte was largely enhanced, and therefore, Li–S battery with HCS could maintain 350 cycles at 0.5C with a capacity of around 800 mAh·g^{-1}.

Solid state electrolyte (SSE) is also a desirable candidate due to its intrinsically high mechanical strength compared to liquid electrolyte [92]. Garnet-type or even some polymer SSEs can process modules above 10 GPa which is theoretically enough to restrain lithium dendrites growth [93, 94]. However, poor electrode–electrolyte interphase hinders the performance of all solid-state lithium metal batteries [95]. Electrodes and high-strength SSEs, especially inorganic electrolytes are basically in point-to-point contact, leading to poor interfacial wettability. It is hard to withstand high current density under large interphase impedance. What's more, lithium dendrites in SSEs system tends to grow in voids at the interphase and along the grain boundary of inorganic SSEs because of low physical barrier, low ion concentration and intensive electric field in these sites, leading to fast protrusion of solid electrolytes and short circuits. Fine-grain size and polished SSEs surface are, therefore, preferable for uniform Li deposition.

Polymer-based electrolytes like poly(ethylene oxide) (PEO) can realize good interfacial contact because of their high flexibility. Additives such as Mg^+ [96] and inorganic Li salts [97, 98] can further enhance the mobile ion concentration and interfacial stability of polymer-based electrolyte. Adding skeleton in polymer is a promising strategy to enhance the performance of SSEs because a hard skeleton ensures mechanical strength while soft polymer improves the interphase contact [99]. Meanwhile, hard skeletons working as fillers can also disrupt the crystallinity of polymers and improve the ionic conductivity of composited SSEs. A SiO_2-aerogel-reinforced composite polymer electrolyte (CPE) with high elastic modulus (around 0.43 GPa) and ion conductivity (around 0.6 mS·cm^{-1} at 30 °C) was reported in 2018 (Fig. 4c) [100]. LFP-Li with SiO_2/CPE could achieve nearly 100% Coulombic efficiency (CE) at 200 cycles with a capacity around 100 mAh·g^{-1} at 0.5C. The Li//Li symmetric cell with SiO_2-aerogel-reinforced CPE could stably operate over 400 cycles without a short circuit at 0.05 mA·cm^{-2}, 0.05 mAh·cm^{-2}. Poor anode/SSE contact can also be relieved by improving interfacial wettability. Interfacial treatments such as coating Al [101], TiO_2 [102] and surface patterned [103] are proved to be effective to avoid bad interfacial contact. Modification of lithium metal anode is also beneficial in regulating the wettability of anode/SSE interphase. Duan et al. [104] composited lithium metal with graphite to change the wettability with garnet-type SSE. Li-C composite anode showed a large contact angle with

the SSE and the interfacial impedance was only 11 $\Omega\cdot cm^2$ compared with that of pure Li/SSE. Huang et al. [105] combined lithium metal and g-C_3N_4 for continuous interfacial contact. The Li-C_3N_4|SSE|Li-C_3N_4 symmetric cells showed 11 $\Omega\cdot cm^2$ at 1.5 mA·cm^{-2}. Formation of Li_3N with favorable ion-conductivity on the anode surface further suppressed dendrites growth and improved the cycling performance.

In summary, nucleation and dendrites growth are two important processes in Li deposition. Homogeneous nucleation and uniform plating are desirable for stable plating/stripping cycling. Electric field, surface wettability, electron concentration, current density, ion distribution and physical force play vital roles in Li nucleation and growth behaviors. Modification directions of lithium dendrites including electrolytes, separators, SEI layers, electrodes and battery facilities thereby focus on these factors, leading to enhanced cycling efficiency and prolonging battery life.

3 Modified 3D porous anodes for lithium metal battery

During a discharge cycle, most nucleation and growth of lithium dendrites occur at the anode side, either on the current collector or self-supported active substance. Therefore, the composition and structure of lithium metal anodes influence greatly on formation of lithium dendrites. Using lithium metal anodes based on porous or hollow materials with surface modification is one of the most effective approaches to improve lithium metal battery with liquid or gel electrolyte. The large specific surface area and internal storage space of the porous matrix provide favorable conditions for restraining lithium dendrites and volume change during the stripping/plating process. Various designs on composition as well as the architectures of porous metal anodes make a positive effect on moderating nucleation and growth of lithium deposition.

3.1 Regulation of lithium nucleation

As mentioned in Sect. 2.1, absolute smooth interphase is desirable for a stable lithium metal anode because of its uniform electric field as well as electron concentration [106]. Ultra-rough surface is more feasible since defects are much easier to be induced rather than be removed. The overall electric field almost remains uniform when the local nucleation electric field resulting from defects distributes everywhere. Dense pores as a kind of "defects" on metal anodes are thereby useful for nucleation modification [107]. Porous skeletons or arrays such as mesh [108] and foam [109] are classical designs of disordered structures.

Wang et al. [110] fabricated 3D Cu skeleton with open unobstructed pores consisting of loose stacking copper powders (Fig. 5a). Spherical lithium deposition was observed inside porous copper, proving its positive effect on attracting lithium. Ryou et al. [111] introduced micro-holes on lithium metal by applying a micro-needle roller on the lithium surface. The side area of micro-holes has a lower resistance compared to another surface because of the removal of native oxide layer and large surface area from vertical striation pattern after micro-needle treatment. SEM images of lithium metal anode after the charging process showed that lithium plated mostly inside vertical striation pattern (Fig. 5b–d). Lu et al. [112] designed a porous current collector composed of copper nanowire (Fig. 5e). In plating cycle, Li^+ is successfully deposited inside copper nanowire without obvious dendrites. Large surface area on porous anodes facilitates the exposure of active sites and further modification of lithiophilic sites on porous precursors. These "nucleation seeds" have good wettability with lithium through chemical reaction or electrostatic attraction, thereby stabilizing lithium metal batteries [113]. Wang et al. [114] combined MXene paper and carbon nano fibers (CNFs) to assemble spheres/sheets mixed porous matrix for stable lithium metal anodes (Fig. 5f). Unique spheres/sheets mixed structure enhances the strength and flexibility of porous matrix. Plenty of polar functional groups on MXene skeletons favor the homogeneous plating of Li^+, leading to uniform lithium nucleation and long-term operation. Xue et al. [115] composited Ag nanowires (AgNWs) on graphene to fabricate a porous host by freeze-drying. AgNWs enhance the wettability and conductivity of metal anodes, promoting lithium deposition inside porous arrays. Full cells with NCM523 achieved 38% capacity retention after 1000 cycles at 10.0C (1.0C = 155 mAh·g^{-1}).

3.2 Regulation of dendrites growth

3.2.1 Current density and force

Porous anode can reduce actual current density thereby inhibiting the growth of lithium dendrites. The biggest characteristic of the porous anode is its ultra-large specific surface area and corresponding large inner space volume. When applying a certain current, the actual current density of an anode with a larger specific surface area will be much smaller than that of an anode with a smaller one. According to Sand's time theory, small current density delays the time when the first dendrite starts to grow. Moreover, the morphology of lithium deposition on porous matrix tends to be spherical or "mossy" other than dendritic under a mild reaction rate resulting from small current density. Amorphous lithium may also occur, which is more resistant to
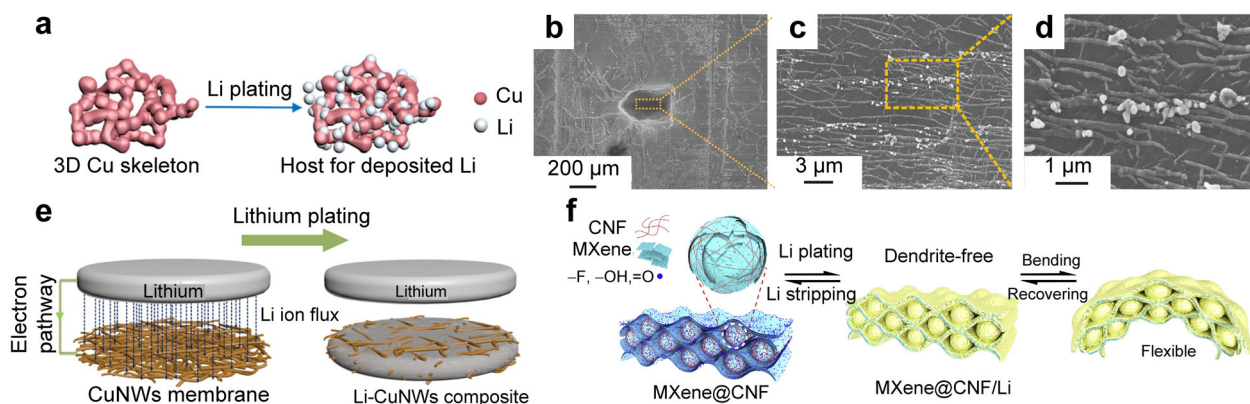
Fig. 5 Modified porous anode for regulating lithium dendrite nucleation. **a** Porous arrays composed of stacked copper powder. Reproduced with permission from Ref. [110]. Copyright 2018, American Chemical Society. **b–d** Porous arrays composed of patterned lithium piece. Reproduced with permission from Ref. [111]. Copyright 2015, WILEY–VCH. **e** Porous current collectors composed of copper nanowires. Reproduced with permission from Ref. [112]. Copyright 2016, American Chemical Society. **f** Spheres/sheets mixed porous anodes composed of CNF and MXene paper. Reproduced with permission from Ref. [114]. Copyright 2020, Elsevier B.V.

organic electrolyte than crystalline lithium. Side reaction is thereby restrained [116]. When lithium plating occurs in porous anode, this unique hollow structure also provides an additional physical barrier on lithium tips [117]. Large space volume inside porous matrix contains violent volume change during lithium stripping/plating cycles, relieving the pressure from dendrites to a separator, thereby stabilizing lithium metal battery [118]. Materials with high strength and toughness such as alloys [119], carbon nanotube [120], and graphene [121] are suitable for fabricating porous anodes. Cheng et al. [122] covered glass fiber on lithium metal to construct a porous barrier for dendrites suppression. What's more, polar ligands on glass fiber evened Li^+ distribution through electrostatic interaction, avoiding Li^+ aggregation on formed lithium nucleus.

3.2.2 Ion distribution

In a conductive matrix, pores with large curvature have high electron concentration and electric field, resulting in Li^+ aggregation and nucleation [123]. The gradient of electron concentration and electric field intensity from the surface of the nucleus to the electrolyte pushes Li^+ to deposit along the opposite direction of the gradient [124]. Therefore, the location and direction of lithium deposition can be controlled. As a short circuit occurs when lithium dendrites penetrate the separator and meet the cathode, changing columnar lithium growth from vertical facing cathode towards horizontal is a method of prolonging battery life too [125]. Zou et al. [126] took the use of etching to fabricate micro-compartmented arrays on Cu current collector (E-Cu) to accommodate lithium deposition. Under the combined effect of upper/lower two insulating polyimide (PI) films and conductive copper walls,

the electric field inside micro-compartments was modified to be mostly vertical to the walls. Therefore, lithium was restrained to deposit only in lateral direction compared to the planar Cu electrode (P-Cu), minimizing the possibility of lithium dendrites protruding the separator and causing a short circuit (Fig. 6a). Improved design of the micro-compartmented arrays was reported by the same research group in 2018 [127]. They alternately stacked the lithium films and graphene oxide (GO) films with designed vertical holes (Fig. 6b). The patterned reduced graphene oxide/Li composite anodes (P-rGO/Li) contributed to horizontal centripetal plating and further enlarged the volume for lithium accommodation.

Interconnected porous structure is beneficial to increase ion transport rate and suppress lithium dendrite growth [128] considering the influence of ion transmission rate on ion concentration. Compared with solid anodes, through-holes in porous anodes provide more ion-conducting channels, thereby reducing polarization and conductive voltage loss [129]. Small pores with large curvature help concentrate the electric field to regulate Li^+ distribution, consequent deposition location as well as direction. Relatively large pores are also needed to obtain sufficient inner space for lithium accommodation. Therefore, ideal porous structure is a combination of various pore sizes. Nevertheless, complex porous structures are difficult to fabricate artificially. Some natural biomass and their processed products have hierarchical fine pore structures [130] such as wood [131], fiber [132] and cotton [133], which can be utilized to fabricate advanced porous materials for stable lithium metal anodes. Jin et al. [134] used bamboo fibers as precursors and fabricated a 3D hierarchical porous carbon host (ZnO@HPC) for stable lithium deposition. Natural bamboo fibers have abundant pores on the surface
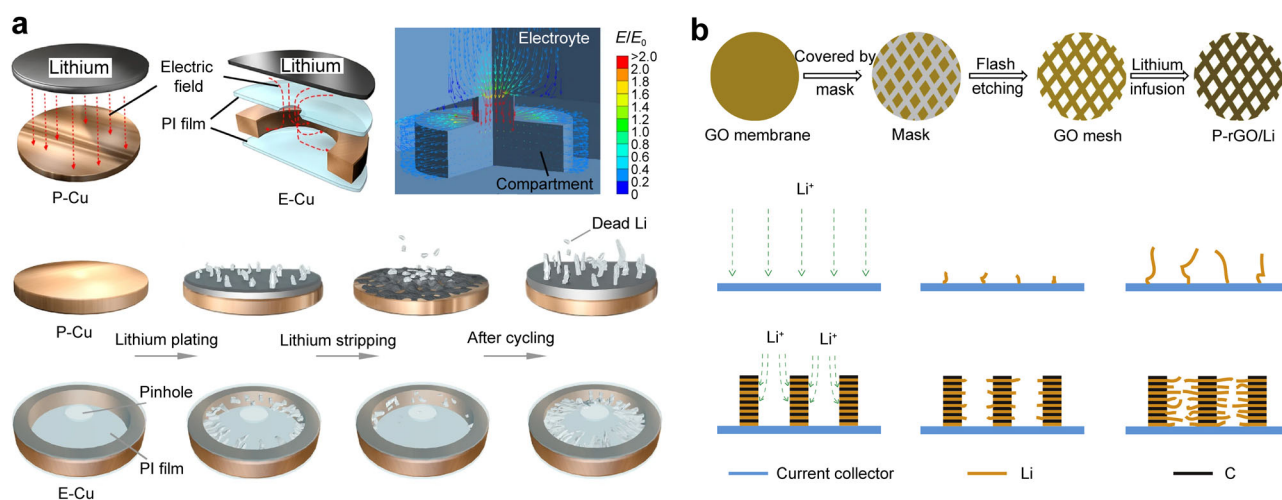
Fig. 6 Advanced porous anode for controlling growth of lithium dendrite. **a** Micro-compartmented Cu collector, where E/E_0 is relative electric field intensity. Reproduced with permission from Ref. [126]. Copyright 2018, Springer Nature. **b** stacked lithium/GO films with vertical holes. Reproduced with permission from Ref. [127]. Copyright 2018, Elsevier B.V.

for water and nutrient transportation. After being treated by KOH at 700 °C, interconnected large pores with diameter of 0.9 μm were uniformly distributed through the fibers. Micropores induced by gas release during activation as well as carbonization treatment were also formed on the large pores' walls, leading to fast ion transportation and portable surface condition for further loading of lithiophilic seeds. ZnO quantum dots were doped in pores to guide lithium deposition. Coulombic efficiency of 25 wt% ZnO@HPC could maintain 95% over 200 cycles at 1 mA·cm^{-2}. Zhang et al. [135] carbonized litchi shells to fabricate hierarchical porous anode for lithium-sulfur batteries. Interconnected macropores in the obtained carbon from litchi shells can form channels that are conducive to ion transition and elements storage, while nanopores can block the movement of polysulfides in the electrolytes. Coulombic efficiency of 60 wt% sulfur contained composite anode could maintain 99% over 100 cycles at 800 mA·g^{-1}.

3.3 Designs of gradient porous anodes for regulating lithium nucleation and growth

Lithium metal anodes usually need to be thick enough to ensure that the anodes have sufficient capacity [136]. Although ion transport condition inside porous host is better than that of the solid bulk anode because of large inner volume, the ion conductivity of porous anodes is still far lower than that of liquid electrolyte [137]. Therefore, ion concentration on the side of porous anodes in contact with the electrolyte is higher than that on the current collector side. Ion transition on the top is also relatively easier. Meanwhile, electron concentration or electric field

intensity on a top surface of a porous host is even a little larger [49]. As a result, Li$^+$ is preferentially reduced on the outmost surface of the porous host, hindering the subsequent movement of Li$^+$ to the depth [138]. In addition, deposited lithium on the surface of a porous host is in direct contact with a corrosive organic electrolyte, leading to serious side reaction, the formation of dead lithium and deterioration of battery life [139]. In consequence, an anode with an evenly porous structure alone cannot fully exert its theoretical effect on suppressing lithium dendrites in the deep charge/discharge process and long-time cycling.

One way to enhance the performance of a porous host is to construct a porous anode with an electron conductive-insulating or lithiophilic-lithiophobic gradient. The electron conductivity of the gradient anode is gradually reduced from current collector side to the outmost surface contacting electrolyte, hindering the electron movement to the surface where free Li$^+$ firstly meets. The lithiophilic–lithiophobic gradient in the same direction attracts the Li$^+$ to the deep anodes, reducing the ion concentration at anode-electrolyte interphase [140]. Therefore, porous gradient anodes restrain dendritic lithium formation on the outside surface but facilitate dense plating from the inside out. The contact area between deposited lithium and the organic electrolyte is greatly reduced, leading to less generation of SEI layer and "dead" lithium [141]. Hong et al. [142] used insulating cellulose fiber (CNF) decorated with SiO$_2$ and highly conductive nanowires (CuNW) to construct an electrical conductivity gradient host for lithium metal anode (Fig. 7a). Resistance of top conductive CuNW layer is 0.1 Ω while that of the insulating CNF layer is 0.9 Ω. Full cell with NCM811 as the cathode (N/P ≈ 5)
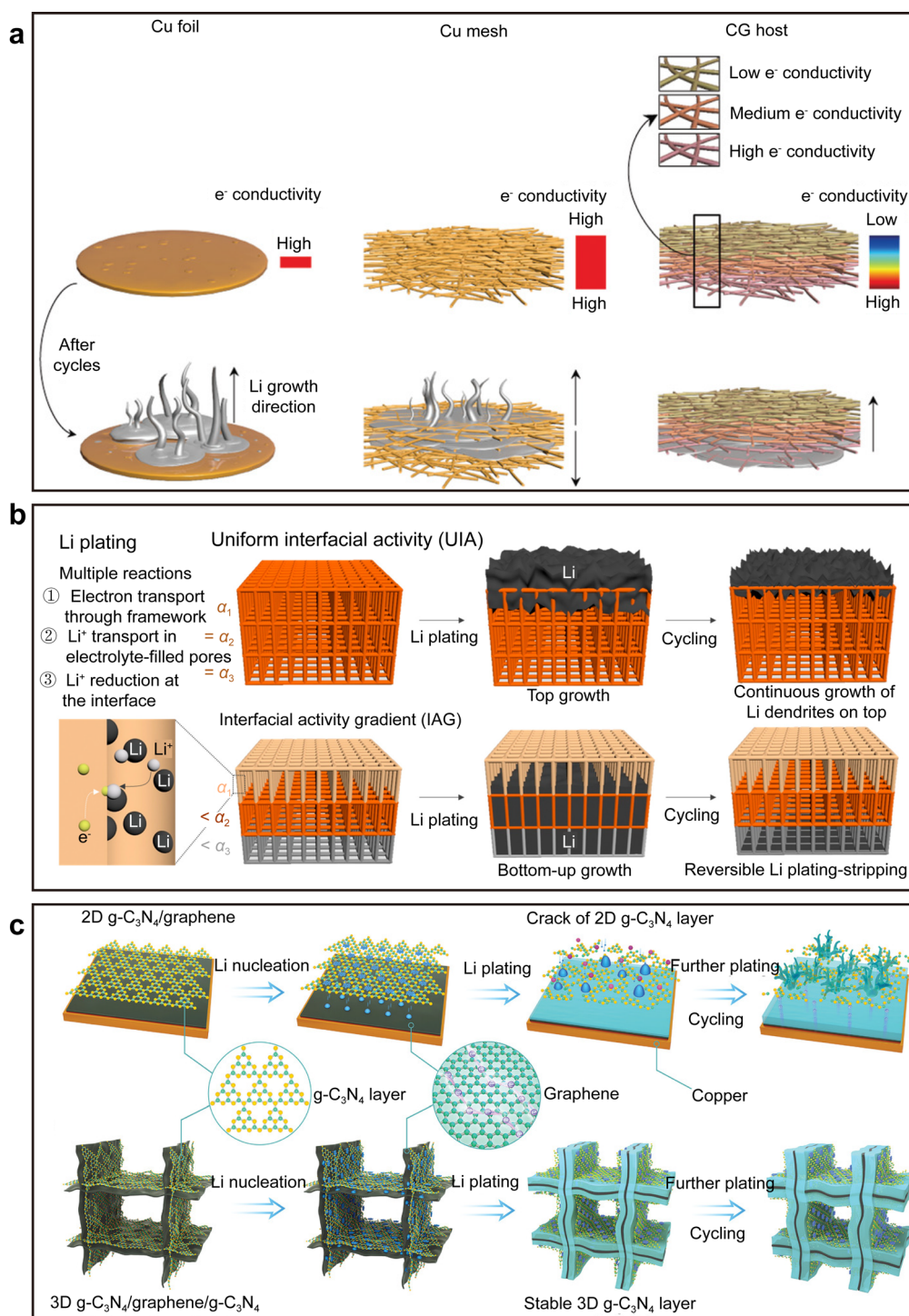
Fig. 7 Conductive-insulating gradient porous anode for long-time duration lithium metal battery. **a** Gradient anode composed of CuNW with SiO$_2$@CNF. Reproduced with permission from Ref. [142]. Copyright 2020, WILEY–VCH. **b** Gradient Ag@Cu with PVDF@Cu. Reproduced with permission from Ref. [143]. Copyright 2020, American Chemical Society. **c** 3D gradient g-C$_3$N$_4$/GO. Reproduced with permission from Ref. [144]. Copyright 2021, WILEY–VCH

maintained 90% capacity retention over 100 cycles. Lithiophilic seeds can also be introduced on conductive layers to increase the effect of attracting Li$^+$. Yun et al. [143] improved the performance of 3D porous copper frameworks by introducing Ag nanolayer and PVDF film to its two sides (Fig. 7b). During discharging, Li$^+$ plates from bottom Ag-blended region to top PVDF-blended region. Symmetric cycling at 1 mA·cm^{-2}, 1 mAh·cm^{-2} can be

maintained voltage hysteresis lower than 100 mV over 260 h. Cycling performance may be further improved by adjusting pore size and distribution. Besides direct addition on porous scaffold, integration of small units with gradient structures into overall porous electrodes can further stabilizing lithium metal anode. Zhai et al. [144] designed a gradient unit by in situ growing an electron insulating but ion conductive g-C_3N_4 layer on graphene oxide. After freeze-drying and calcination, these units were assembled to form a 3D porous matrix (Fig. 7c). Although g-C_3N_4 can serve as nucleation sites because N is lithiophilic, further lithium deposition is inclined to happen inside g-C_3N_4/GO transition layer because of lower structure fluctuation and larger adsorption energy. Full cell with 3D g-C_3N_4 as anode and LFP as cathode (N/P $\approx$ 0.45) maintained 90% capacity retention for 200 cycles at 0.5C. Anode-free full cell with high-loading LFP (3.5 mAh·cm^{-2}) could also achieve 40 cycles with CE over 99.3% at 0.2C.

In summary, 3D porous anode is a promising design for a stable lithium metal battery. The biggest characteristics of porous anodes are large specific surface area and consequently inner space. Compared to other optimization methods such as electrolytes additives, SSEs, coated separators, or artificial SEI layer, porous anode can significantly decrease current density to delay "Sand's time" occurrence and accommodate large volume change during the lithium plating/stripping process. Moreover, a large surface area provides sufficient sites for subtle properties modification such as "nucleation seeds" and electric field. Porous anodes based on the mechanically strong matrix can also withstand high physical stress from lithium dendrites and maintain battery stability. Further enhancement of 3D porous anodes' life can be achieved by construction of conductive or lithiophilic gradient.

4 Conclusion

In this review, we discuss the mechanism and strategies to stabilize lithium metal battery which is one of the most promising candidates for next-generation storage devices. A surface-modified porous matrix is a hopeful material for high-energy-density lithium metal anode. Its large surface area and internal space provide a stable platform for lithium deposition. Further improvement of a porous host can be achieved by controllable surface adjustment. Particularly, the porous gradient anode further makes a full use of the porous structure. It enables repeated Li plating/ stripping and thus achieves superior cycling performance. Nevertheless, the disadvantages of porous anodes cannot be ignored. The development of gradient porous anode also needs further optimization and efforts. Details are discussed below.

Firstly, the relatively large thickness and weight of porous anodes hinder the realization of high-energy-density of lithium metal batteries. Thickness less than 50 μm is more desirable for lithium metal anodes. Large surface area of porous anodes promotes the contact area between lithium metal and electrolyte, resulting in additional side reactions and capacity loss. What's more, sufficient interfacial contact between 3D porous matrix and SSEs is hardly obtainable, especially in inorganic solid electrolyte system. Since SSEs are effective in avoiding leakage, flammability of lithium metal battery and suppressing lithium dendrites through intrinsic strength compared to liquid electrolytes, it is essential to overcome the challenges of poor interfacial wettability [145]. Assembling porous anodes inside SSEs is a possible solution [146], while further research on stability of these novel designs is still necessary.

Optimization of gradient porous anodes should consider the following aspects. During electrochemical plating, an electron-conductivity gradient could guide the nucleation position of lithium metal. Sufficient ion conduction is also needed to ensure the penetration of Li$^+$ in lithium electroplating process. Based on the above two points, complex requirements are put forward for the porosity of material. Small holes with large curvature aggregate more electron charge and electric field with strong attraction to lithiumion, realizing the regulation of plating sites at the structural level. Large holes provide fluent ionic flux channels and sufficient space to accommodate volume change during cycles. The precise hole size, ratio of "small" to "large" and the gradient of the hierarchical structure still need further discussion. Here we summarize several pore parameters and corresponding cycling performance from several reports in Table 1 [35, 38, 42, 59, 109, 115, 131, 135, 144, 147, 157], hoping that it can provide some references for the future designs of porous materials. Moreover, the lithiophilic-lithiophobic gradient can eliminate the mossy Li corrosion layer at the interphase. The gradient porous materials considering the above aspects can basically meet the conditions of suppressing lithium dendrite formation.

What's more, the physical realization of gradients in electrodes is crucial, especially in thin electrodes. Most gradient designs are achieved by separating the whole materials into a few parts followed by different treatments and orderly arrangements. It is hard to obtain a continuous gradient of electron conductivity or lithiophilic sites which is theoretically more desirable for uniform lithium deposition. Moreover, ultrathin anodes and corresponding low negative/positive electrode capacity (N/P) ratio is essential to ensure the high energy density of lithium metal batteries. Achieving gradients in thinner materials presents a new technical challenge and further efforts are needed on

Table 1 Details of modified porous anodes for lithium metal battery

Brief description	Information of pores	Cycling performance	Refs.
Cu(PI)@Sb	2–90 nm, SSA = 1.9303 $m^2 \cdot g^{-1}$	Half cell: 3 mA·cm^{-2}, 3 mAh·cm^{-2}, CE ≈ 98.5%, 120 cycles (60 ul, 1 mol·L^{-1} LiFTSI in DOL/DME with 2 wt% LiNO$_3$)	[35]
		Full cell: Li$_x$Cu(PI)@Sb‖LFP, 0.5C (4 mA·cm^{-2}), N/P ≈ 1.5, 150 cycles, 91.23% capacity retention	
Oxygen and nitrogen co-doped porous carbon granules (ONPCGs)	0.5–4 nm, SSA$_{bet}$ = 2386.5 $m^2 \cdot g^{-1}$, pore volume = 1.3 $cm^3 \cdot g^{-1}$	Half cell: 2 mA·cm^{-2}, 2 mAh·cm^{-2}, CE ≈ 99.83%, 350 cycles (4 mol·L^{-1} LiFTSI in DME)	[38]
ZnO nanosheets on Ni foam	1–5 μm	Half cell: 1 mA·cm^{-2}, 1 mAh·cm^{-2}, CE ≈ 98.5%, 150 cycles (1 mol·L^{-1} LiFTSI in DOL/DME with 1 wt% LiNO$_3$);	[42]
		Full cell: LZNF‖LFP, 0.5C (1.0C = 85 mAh·g^{-1}), N/P ≈ 27, 200 cycles (1 mol·L^{-1} LiPF$_6$ in EC/EMC/DMC)	
2D Ti$_3$C$_2$T$_x$ MXene stacks on Li metal	< 100 nm, SSA = 5.61 $m^2 \cdot g^{-1}$, pore volume = 0.036 $cm^3 \cdot g^{-1}$	Full cell: ILC-Li‖NMC532, 0.2C/0.5C, N/P ≈ 3, 200 cycles, 83% capacity retention (1 mol·L^{-1} LiPF$_6$ in EC:EMC = 3:7 with 2 wt% VC)	[59]
CNTs/graphene foam (LPM-3D rebar GF)	∼ 5 nm, SSA$_{bet}$ = 42.032 $m^2 \cdot g^{-1}$	Half cell: 5 mA·cm^{-2}, 10 mAh·cm^{-2}, CE ≈ 98%, 120 cycles (80 μl, 1 mol·L^{-1} LiFTSI in DOL/DME with 2 wt% LiNO$_3$)	[109]
Silver-nanowire graphene host (3D-AGBN)	3 μm, SSA$_{bet}$ = 19.9 $m^2 \cdot g^{-1}$	Half cell (pre-lithiated 12 mAh·cm^{-2}): 1 mA·cm^{-2}, 6 mAh·cm^{-2}, CE ≈ 97.3%, 50 cycles (1 mol·L^{-1} LiFTSI in DOL/DME)	[115]
		Full cell (pre-lithiated 12 mAh·cm^{-2}): Li@3D-AGBN‖NCM523, 10.0C (1.0C = 155 mAh·g^{-1}), N/P ≈ 52, 1000 cycles, 38% capacity retention (1 mol·L^{-1} LiPF$_6$ and 0.1 mol·L^{-1} LiFTSI in EC/DMC/EMC)	
Nanowood-protected LMBs	∼ 2.3 nm, SSA$_{bet}$ = 33 $m^2 \cdot g^{-1}$	Half cell (nanowood-protected Li): 1 mA·cm^{-2}, 1 mAh·cm^{-2}, CE ≈ 99%, 400 cycles (1 mol·L^{-1} LiFTSI in DOL/DME with 0.1 mol·L^{-1} LiNO$_3$)	[131]
		Full cell: nanowood-protected Li‖LFP, 0.5C (1.0C = 174 mAh·g^{-1}), 800 cycles (50 μl, 1 mol·L^{-1} LiFTSI in DOL/DME)	
Litchi shells-derived activated carbon/ 60 wt% sulfur composite for Li–S battery	1–2 nm (BJH size distribution), 295 $m^2 \cdot g^{-1}$	800 mA·g^{-1}, over 800 cycles, 51% capacity retention (1 mol·L^{-1} LiFTSI in DOL/DME)	[135]
3D g-C$_3$N$_4$/graphene composite anodes	3.23 $cm^3 \cdot g^{-1}$; 241.73 $m^2 \cdot g^{-1}$	Half-cell: 1 mA·cm^{-2}, 1 mAh·cm^{-2}, CE ≈ 99%, 500 cycles (25 μl, 1 mol·L^{-1} LiFTSI in DOL/DME with 1 wt% LiNO$_3$)	[144]
		Full cell: Li-3D g-C$_3$N$_4$/G/g-C$_3$N$_4$‖LFP, 0.5C (1.0C = 2.2 mAh·cm^{-2}), N/P ≈ 0.45, 200 cycles (20 μl, 1 mol·L^{-1} LiPF$_6$ in EC/EMC with 2 wt% VC)	
3D porous Cu mesh dealloyed from Cu$_{0.64}$Zn$_{0.36}$	200 nm–2 μm 0.5 $m^2 \cdot g^{-1}$	Half cell: 1 mA·cm^{-2}, 1 mAh·cm^{-2}, CE ≈ 97%, 140 cycles (40 μl, 1 mol·L^{-1} LiFTSI in DOL/DME with 1 wt% LiNO$_3$)	[147]
		Full cell: 3D porous Cu‖LFP, 0.5C, N/P ≈ 10, 300 cycles, 89.7% capacity retention	
Unstacked graphene framework	0.5–10 nm, SSA$_{bet}$:1666 $m^2 \cdot g^{-1}$, pore volume: 1.65 $cm^3 \cdot g^{-1}$	Half cell: 2 mA·cm^{-2}, 1 mAh·cm^{-2}, CE ≈ 97%, 50 cycles (1 mol·L^{-1} LiFTSI in DOL/DME)	[148]
Graphene nested Cu foam (CuFG)	Macropores, ∼ 5 μm	Half cell: 1 mA·cm^{-2}, 1 mAh·cm^{-2}, CE ≈ 98%, 200 cycles (100 μl, 1 mol·L^{-1} LiFTSI in DOL/DME with 1 wt% LiNO$_3$)	[149]

Table 1 continued

Brief description	Information of pores	Cycling performance	Refs.
3D hollow carbon fiber from cotton	0.6–2.5 nm, $SSA = 140.1$ m$^2 \cdot$g^{-1}	Half cell (pre-lithiated 6 mAh$\cdot$cm^{-2}): 1 mA$\cdot$cm^{-2}, 2 mAh$\cdot$cm^{-2}, CE $\approx$ 99.5%, 240 cycles (1 mol$\cdot$L^{-1} LiFTSI in DOL/DME with 1 wt% LiNO$_3$)	[150]
		Full cell: 3D-HCFs@Li||LFP, 0.5C (1.0C = 1 mA$\cdot$cm^{-2}), N/P $\approx$ 3, 200 cycles, 91.3% capacity retention	
Porous CuZn alloy	1–5 μm	Half cell (pre-lithiated 2 mAh$\cdot$cm^{-2}): 1 mA$\cdot$cm^{-2}, 1 mAh$\cdot$cm^{-2}, CE $\approx$ 97.8%, 250 cycles (80 μl, 1 mol$\cdot$L^{-1} LiPF$_6$ in EC/EMC/DMC)	[151]
		Full cell: CuZn-Li||NMC811, 1.0C (1.0C = 170 mAh$\cdot$g^{-1}), N/P $\approx$ 4, 500 cycles, (80 μl, 1 mol$\cdot$L^{-1} LiPF6 in EC/EMC/DMC)	
N-doped amorphous Zn-carbon fibers	$SSA_{bet} = 74.7$ m$^2 \cdot$g^{-1}	Half cell (pre-lithiated 6 mAh$\cdot$cm^{-2}): 1 mA$\cdot$cm^{-2}, 1 mAh$\cdot$cm^{-2}, CE $\approx$ 99%, 800 cycles (50 μl, 1 mol$\cdot$L^{-1} LiFTSI in DOL/DME with 2 wt% LiNO$_3$)	[152]
		Full cell (pre-lithiated 6 mAh$\cdot$cm^{-2}): CC-Zn-CMFs-Li||LFP, 1.0C (1.0C = 170 mAh$\cdot$g^{-1}), N/P $\approx$ 7.5, 200 cycles (50 μl, 1 mol$\cdot$L^{-1} LiPF$_6$ in EC/ DMC)	
Al-Al$_x$O$_y$-C-25%	2–15 nm $SSA_{bet} > 400$ m$^2 \cdot$g^{-1}	Half cell: 1 mA$\cdot$cm^{-2}, 1 mAh$\cdot$cm^{-2}, CE $\approx$ 99.5%, 150 cycles (100 μl, 1 mol$\cdot$L^{-1} LiFTSI in DOL/DME)	[153]
		Full cell: CC-Zn-CMFs-Li||NMC-811, 0.5C (1.0C = 120 mAh$\cdot$g^{-1}), N/P $\approx$ 2.7, 300 cycles, 94% capacity retention (40 μl, 1 mol$\cdot$L^{-1} LiPF$_6$ in EC/DEC/EMC)	
Li metal-graphene oxide host foils (eGF)	Effective pore sizes, $\sim$ 2 or $\sim$ 3 nm, $SSA_{bet} = 338$ m$^2 \cdot$g^{-1}	Pouch full cell: 20-μm-thick Li@eGF||LFP, 0.5C (1.0C = 150 mAh$\cdot$g^{-1}), N/P $\approx$ 1.3, 200 cycles, 94% capacity retention (30 μl, 1 mol$\cdot$L^{-1} LiPF$_6$ in EC/DEC with 1 wt% VC and 10 wt% FEC)	[154]
Ni-Co hollow prisms@carbon fibers	Mesopores $SSA_{bet} = 215.7$ m$^2 \cdot$g^{-1}	Full cell: Li-NCH@CF||LFP, 1.0C (1.0C = 169 mAh$\cdot$g^{-1}), N/P $\approx$ 6, 150 cycles, 90% capacity retention (60 μl, 1 mol$\cdot$L^{-1} LiPF$_6$ in EC/DEC/EMC)	[155]
Lignin carbon membranes (OLCMs)	$\sim$ 0.9 nm $SSA_{bet} = 424$ m$^2 \cdot$g^{-1}	Half cell: 1 mA$\cdot$cm^{-2}, 1 mAh$\cdot$cm^{-2}, CE $\approx$ 98%, 230 cycles (40 μl, 1 mol$\cdot$L^{-1} LiFTSI in DOL/DME with 1 wt% LiNO$_3$)	[156]
		Full cell: OLCM@Li||NMC811, 1.0C (1.0C = 0.8 mAh$\cdot$cm^{-2}), N/P $\approx$ 7.5, 150 cycles, 88% capacity retention (1 mol$\cdot$L^{-1} LiPF$_6$ in EC/DEC with 2 wt% VC)	
Fluorinated porous copper powder	100–500 nm, $SSA_{bet} = 5.21$ m$^2 \cdot$g^{-1}	Full cell: LiF-Li-Cu||NCM111, 0.5C (1.0C = 170 mAh$\cdot$g^{-1}), 300 cycles, 83% capacity retention (1 mol$\cdot$L^{-1} LiPF$_6$ in EC/DEC)	[157]

advanced porous lithium metal anodes [124]. Besides, current designs of gradient porous anodes are almost fabricated in labs. Low-cost and efficient manufacturing process is under urgent need for large-scale applications in the markets.

Porous anode is expected to solve the problems in the practical application of lithium metal battery and has a broad prospect. We are committed to achieving higher energy density and more stable cycling performance through the designs of porous anode. High-energy-density storage devices are increasingly demanded and an efficient manufacturing process is essential for large-scale applications in the industry. Under the constant efforts from researchers all over the world, stable, safe and efficient lithium metal battery can be commercially available in the near future.

Declarations

Conflict of interests The authors declare that they have no conflict of interests.

References

[1] Goodenough JB. Energy storage materials: a perspective. Energy Storage Mater. 2015;1:158.

[2] Evarts EC. Lithium batteries to the limits of lithium. Nature. 2015;526(7575):93.

[3] Winter M, Barnett B, Xu K. Before Li ion batteries. Chem Rev. 2018;118(23):11433.

[4] Guo YP, Li HQ, Zhai TY. Reviving lithium-metal anodes for next-generation high-energy batteries. Adv Mater. 2017; 29(29):1700007.

[5] Kennedy T, Mullane E, Geaney H, Osiak M, O'Dwyer C, Ryan KM. High-performance germanium nanowire-based lithium-ion battery anodes extending over 1000 cycles through in situ formation of a continuous porous network. Nano Lett. 2014;14(2):716.

[6] Whittingham MS. Lithium batteries: 50 years of advances to address the next 20 years of climate issues. Nano Lett. 2020; 20(12):8435.

[7] Anonymous. Battery revolution to evolution. Nat Energy. 2019; 4(11): 893.

[8] Eftekhari A. On the theoretical capacity/energy of lithium batteries and their counterparts. ACS Sustain Chem Eng. 2019; 7(4):3684.

[9] Li B, Wang Y, Yang SB. A material perspective of rechargeable metallic lithium anodes. Adv Energy Mater. 2018;8(13): 1702296.

[10] Tarascon JM, Armand M. Issues and challenges facing rechargeable lithium batteries. Nature. 2001;414(6861):359.

[11] Cheng XB, Zhang R, Zhao CZ, Zhang Q. Toward safe lithium metal anode in rechargeable batteries: a review. Chem Rev. 2017;117(15):10403.

[12] Bruce PG, Freunberger SA, Hardwick LJ, Tarascon JM. Li–O_2 and Li–S batteries with high energy storage. Nature Mater. 2012;11(1):19.

[13] Jäckle M, Groß A. Microscopic properties of lithium, sodium, and magnesium battery anode materials related to possible dendrite growth. J Chem Phys. 2014;141(17):174710.

[14] Ling C, Banerjee D, Matsui M. Study of the electrochemical deposition of Mg in the atomic level: why it prefers the non-dendritic morphology. Electrochim Acta. 2012;76:270.

[15] Goodenough JB, Kim Y. Challenges for rechargeable batteries. J Power Sour. 2011;196(16):6688.

[16] Odziemkowski M. An electrochemical study of the reactivity at the lithium electrolyte/bare lithium metal interface. J Electrochem Soc. 1992;139(11):3063.

[17] Zhou H, Yu S, Liu H, Liu P. Protective coatings for lithium metal anodes: recent progress and future perspectives. J Power Sour. 2020;450:227632.

[18] Zhang LQ, Yang TT, Du CC, Liu QN, Tang YS, Zhao J, Wang BL, Chen TW, Sun Y, Jia P, Li H, Geng L, Chen JZ, Ye HJ, Wang ZF, Li YS, Sun HM, Li XM, Dai QS, Tang YF, Peng QM, Shen TD, Zhang SL, Zhu T, Huang JY. Lithium whisker growth and stress generation in an in situ atomic force microscope-environmental transmission electron microscope set-up. Nat Nanotechnol. 2020;15(2):94.

[19] Cheng XB, Zhang R, Zhao CZ, Wei F, Zhang JG, Zhang Q. A review of solid electrolyte interphases on lithium metal anode. Adv Sci. 2016;3(3):1500213.

[20] Gunnarsdóttir AB, Amanchukwu CV, Menkin S, Grey CP. Noninvasive in situ NMR study of "dead lithium" formation and lithium corrosion in full-cell lithium metal batteries. J Am Chem Soc. 2020;142(49):20814.

[21] Jin C, Liu T, Sheng O, Li M, Liu T, Yuan Y, Nai J, Ju Z, Zhang W, Liu Y, Wang Y, Lin Z, Lu J, Tao X. Rejuvenating dead lithium supply in lithium metal anodes by iodine redox. Nat Energy. 2021;6(4):378.

[22] Li HY, Yamaguchi T, Matsumoto S, Hoshikawa H, Kumagai T, Okamoto NL, Ichitsubo T. Circumventing huge volume strain in alloy anodes of lithium batteries. Nat Commun. 2020; 11(1):1584.

[23] Kushima A, So KP, Su C, Bai P, Kuriyama N, Maebashi T, Fujiwara Y, Bazant MZ, Li J. Liquid cell transmission electron microscopy observation of lithium metal growth and dissolution: root growth, dead lithium and lithium flotsams. Nano Energy. 2017;32:271.

[24] Steiger J, Kramer D, Mönig R. Microscopic observations of the formation, growth and shrinkage of lithium moss during electrodeposition and dissolution. Electrochim Acta. 2014;136:529.

[25] Wu F, Maier J, Yu Y. Guidelines and trends for next-generation rechargeable lithium and lithium-ion batteries. Chem Soc Rev. 2020;49(5):1569.

[26] Liu SF, Wang XL, Xie D, Xia XH, Gu CD, Wu JB, Tu JP. Recent development in lithium metal anodes of liquid-state rechargeable batteries. J Alloys Compd. 2018;730:135.

[27] Liu J, Bao Z, Cui Y, Dufek EJ, Goodenough JB, Khalifah P, Li Q, Liaw BY, Liu P, Manthiram A, Meng YS, Subramanian VR, Toney MF, Viswanathan VV, Whittingham MS, Xiao J, Xu W, Yang J, Yang XQ, Zhang JG. Pathways for practical high-energy long-cycling lithium metal batteries. Nat Energy. 2019; 4(3):180.

[28] Ely DR, García RE. Heterogeneous nucleation and growth of lithium electrodeposits on negative electrodes. J Electrochem Soc. 2013;160(4):662.

[29] Jana A, Woo SI, Vikrant KSN, García RE. Electrochemomechanics of lithium dendrite growth. Energy Environ Sci. 2019; 12(12):3595.

[30] Aguesse F, Manalastas W, Buannic L, Lopez del Amo JM, Singh G, Llordés A, Kilner J. Investigating the dendritic growth during full cell cycling of garnet electrolyte in direct contact with Li metal. ACS Appl Mater Interfaces. 2017;9(4): 3808.

[31] Tian HK, Xu B, Qi Y. Computational study of lithium nucleation tendency in $Li_7La_3Zr_2O_{12}$ (LLZO) and rational design of interlayer materials to prevent lithium dendrites. J Power Sour. 2018;392:79.

[32] Harry KJ, Hallinan DT, Parkinson DY, MacDowell AA, Balsara NP. Detection of subsurface structures underneath dendrites formed on cycled lithium metal electrodes. Nature Mater. 2014;13(1):69.

[33] Meng Q, Deng B, Zhang H, Wang B, Zhang W, Wen Y, Ming H, Zhu X, Guan Y, Xiang Y, Li M, Cao G, Yang Y, Peng H, Zhang H, Huang Y. Heterogeneous nucleation and growth of electrodeposited lithium metal on the basal plane of single-layer graphene. Energy Storage Mater. 2019;16:419.

[34] Han F, Westover AS, Yue J, Fan X, Wang F, Chi M, Leonard DN, Dudney NJ, Wang H, Wang C. High electronic conductivity as the origin of lithium dendrite formation within solid electrolytes. Nat Energy. 2019;4(3):187.

[35] Wang J, Wang M, Chen F, Li Y, Zhang L, Zhao Y, Chen C. In-situ construction of lithiophilic interphase in vertical micro-channels of 3D copper current collector for high performance lithium-metal batteries. Energy Storage Mater. 2021; 34:22.

[36] Wang J, Wang H, Xie J, Yang A, Pei A, Wu CL, Shi F, Liu Y, Lin D, Gong Y, Cui Y. Fundamental study on the wetting property of liquid lithium. Energy Storage Mater. 2018;14:345.

[37] Niu CJ, Pan HL, Xu W, Xiao J, Zhang JG, Luo LL, Wang CM, Mei DH, Meng JS, Wang XP, Liu Z, Mai LQ, Liu J. Self-smoothing anode for achieving high-energy lithium metal batteries under realistic conditions. Nat Nanotechnol. 2019;14(6):594.

[38] Liu Y, Qin X, Zhang S, Huang Y, Kang F, Chen G, Li B. Oxygen and nitrogen co-doped porous carbon granules enabling dendrite-free lithium metal anode. Energy Storage Mater. 2019;18:320.

[39] Yan K, Lu Z, Lee HW, Xiong F, Hsu PC, Li Y, Zhao J, Chu S, Cui Y. Selective deposition and stable encapsulation of lithium through heterogeneous seeded growth. Nat Energy. 2016;1(3):16010.

[40] Tian R, Chen RH, Xu ZM, Wan SL, Guan L, Duan HN, Li H, Zhu H, Sun D, Liu HZ. Electrodeposition behavior of lithium metal on carbon substrates with surface silvering. Carbon. 2019;152:503.

[41] Liu FF, Jin ZZ, Hu ZX, Zhang ZW, Liu W, Yu Y. Constructing Co_3O_4 nanowires on carbon fiber film as a lithiophilic host for stable lithium metal anodes. Chem Asian J. 2020;15(7):1057.

[42] Zhao F, Zhou XF, Deng W, Liu ZP. Entrapping lithium deposition in lithiophilic reservoir constructed by vertically aligned ZnO nanosheets for dendrite-free Li metal anodes. Nano Energy. 2019;62:55.

[43] Park MG, Sung GK, Sung NE, Kim JH, Park CM. Partially reversible Li_2O formation in ZnO: a critical finding supporting realization of highly reversible metal oxide electrodes. J Power Sour. 2016;328:607.

[44] Rosso M, Gobron T, Brissot C, Chazalviel JN, Lascaud S. Onset of dendritic growth in lithium/polymer cells. J Power Sour. 2001;97:804.

[45] Sand HJS. On the concentration at the electrodes in a solution with special reference to the liberation of hydrogen by electrolysis of a mixture of copper sulphate and sulphuric acid. London Edinburgh Dublin Philos Mag J Sci. 1901;1(1):45.

[46] Bai P, Li J, Brushett FR, Bazant MZ. Transition of lithium growth mechanisms in liquid electrolytes. Energy Environ Sci. 2016;9(10):3221.

[47] Bai P, Guo JZ, Wang M, Kushima A, Su L, Li J, Brushett FR, Bazant MZ. Interactions between lithium growths and nanoporous ceramic separators. Joule. 2018;2(11):2434.

[48] Li L, Basu S, Wang Y, Chen Z, Hundekar P, Wang B, Shi J, Shi Y, Narayanan S, Koratkar N. Self-heating-induced healing of lithium dendrites. Science. 2018;359(6383):1513.

[49] Zou P, Chiang SW, Li J, Wang Y, Wang X, Wu D, Nairan A, Kang F, Yang C. Ni@Li_2O co-axial nanowire based reticular anode: tuning electric field distribution for homogeneous lithium deposition. Energy Storage Mater. 2019;18:155.

[50] Yang H, Li J, Sun Z, Fang R, Wang DW, He K, Cheng HM, Li F. Reliable liquid electrolytes for lithium metal batteries. Energy Storage Mater. 2020;30:113.

[51] Zheng H, Xie Y, Xiang H, Shi P, Liang X, Xu W. A bifunctional electrolyte additive for separator wetting and dendrite suppression in lithium metal batteries. Electrochim Acta. 2018;270:62.

[52] Wang H, Matsui M, Kuwata H, Sonoki H, Matsuda Y, Shang X, Takeda Y, Yamamoto O, Imanishi N. A reversible dendrite-free high-areal-capacity lithium metal electrode. Nat Commun. 2017;8(1):15106.

[53] Ren X, Chen S, Lee H, Mei D, Engelhard MH, Burton SD, Zhao W, Zheng J, Li Q, Ding MS, Schroeder M, Alvarado J, Xu K, Meng YS, Liu J, Zhang JG, Xu W. Localized

[54] Shen K, Wang Z, Bi X, Ying Y, Zhang D, Jin C, Hou G, Cao H, Wu L, Zheng G, Tang Y, Tao X, Lu J. Magnetic field–suppressed lithium dendrite growth for stable lithium-metal batteries. Adv Energy Mater. 2019;9(20):1900260.

[55] Wang A, Deng Q, Deng L, Guan X, Luo J. Eliminating tip dendrite growth by Lorentz force for stable lithium metal anodes. Adv Funct Mater. 2019;29(25):1902630.

[56] Family F. Fractal concepts in surface growth. J Stat Phys. 1996;83(5):1255.

[57] Wang J, Hu Y, Yang B, Wang X, Qin J, Cao M. Mechanochemistry-induced biaxial compressive strain engineering in MXenes for boosting lithium storage kinetics. Nano Energy. 2021;87:106053.

[58] Peled E, Golodnitsky D, Ardel G. Advanced model for solid electrolyte interphase electrodes in liquid and polymer electrolytes. J Electrochem Soc. 1997;144(8):208.

[59] Chen X, Shang M, Niu J. Inter-layer-calated thin Li metal electrode with improved battery capacity retention and dendrite suppression. Nano Lett. 2020;20(4):2639.

[60] Liu Y, Lin D, Yuen PY, Liu K, Xie J, Dauskardt RH, Cui Y. An artificial solid electrolyte interphase with high Li-ion conductivity, mechanical strength, and flexibility for stable lithium metal anodes. Adv Mater. 2017;29(10):1605531.

[61] Chen XR, Yao YX, Yan C, Zhang R, Cheng XB, Zhang Q. A diffusion-reaction competition mechanism to tailor lithium deposition for lithium-metal batteries. Angew Chem Int Ed. 2020;59:7743.

[62] Zhang XQ, Chen X, Cheng XB, Li BQ, Shen X, Yan C, Huang JQ, Zhang Q. Highly stable lithium metal batteries enabled by regulating the solvation of lithium ions in nonaqueous electrolytes. Angew Chem Int Ed. 2018;57(19):5301.

[63] Xue W, Shi Z, Huang M, Feng S, Wang C, Wang F, Lopez J, Qiao B, Xu G, Zhang W, Dong Y, Gao R, Shao-Horn Y, Johnson JA, Li J. FSI-inspired solvent and "full fluorosulfonyl" electrolyte for 4 V class lithium-metal batteries. Energy Environ Sci. 2020;13(1):212.

[64] Xue W, Huang M, Li Y, Zhu YG, Gao R, Xiao X, Zhang W, Li S, Xu G, Yu Y, Li P, Lopez J, Yu D, Dong Y, Fan W, Shi Z, Xiong R, Sun CJ, Hwang I, Lee WK, Shao-Horn Y, Johnson JA, Li J. Ultra-high-voltage Ni-rich layered cathodes in practical Li metal batteries enabled by a sulfonamide-based electrolyte. Nat Energy. 2021;6(5):495.

[65] Zhang P, Zhu J, Wang M, Imanishi N, Yamamoto O. Lithium dendrite suppression and cycling efficiency of lithium anode. Electrochem Commun. 2018;87:27.

[66] Suo L, Xue W, Gobet M, Greenbaum SG, Wang C, Chen Y, Yang W, Li Y, Li J. Fluorine-donating electrolytes enable highly reversible 5-V-class Li metal batteries. Proc Natl Acad Sci. 2018;115(6):1156.

[67] Yuan Y, Wu F, Chen G, Bai Y, Wu C. Porous LiF layer fabricated by a facile chemical method toward dendrite-free lithium metal anode. J Energy Chem. 2019;37:197.

[68] Guo J, Wen Z, Wu M, Jin J, Liu Y. Vinylene carbonate–$LiNO_3$: a hybrid additive in carbonic ester electrolytes for SEI modification on Li metal anode. Electrochem Commun. 2015;51:59.

[69] Yoon S, Lee J, Kim SO, Sohn HJ. Enhanced cyclability and surface characteristics of lithium batteries by Li–Mg co-deposition and addition of HF acid in electrolyte. Electrochim Acta. 2008;53(5):2501.

[70] Ishikawa M, Yoshitake S, Morita M, Matsuda Y. In situ scanning vibrating electrode technique for the characterization

of interface between lithium electrode and electrolytes containing additives. J Electrochem Soc. 1994;141:159.

[71] Jin D, Roh Y, Jo T, Ryou MH, Lee H, Lee YM. Robust cycling of ultrathin Li metal enabled by nitrate-preplanted Li powder composite. Adv Energy Mater. 2021;11(18):2003769.

[72] Ding F, Xu W, Chen X, Zhang J, Shao Y, Engelhard MH, Zhang Y, Blake TA, Graff GL, Liu X, Zhang JG. Effects of cesium cations in lithium deposition via self-healing electrostatic shield mechanism. J Phys Chem C. 2014;118(8):4043.

[73] Ding F, Xu W, Graff GL, Zhang J, Sushko ML, Chen XL, Shao YY, Engelhard M, Nie ZM, Xiao J, Liu XJ, Sushko PV, Liu J, Zhang JG. Dendrite-free lithium deposition via self-healing electrostatic shield mechanism. J Am Chem Soc. 2013;135(11):4450.

[74] Xu X, Wen Z, Yang X, Chen L. Dense nanostructured solid electrolyte with high Li-ion conductivity by spark plasma sintering technique. Mater Res Bull. 2008;43(8):2334.

[75] Wan J, Xie J, Mackanic DG, Burke W, Bao Z, Cui Y. Status, promises, and challenges of nanocomposite solid-state electrolytes for safe and high performance lithium batteries. Mater Today Nano. 2018;4:1.

[76] Lee YG, Fujiki S, Jung C, Suzuki N, Yashiro N, Omoda R, Ko DS, Shiratsuchi T, Sugimoto T, Ryu S, Ku JH, Watanabe T, Park Y, Aihara Y, Im D, Han IT. High-energy long-cycling all-solid-state lithium metal batteries enabled by silver–carbon composite anodes. Nat Energy. 2020;5(4):299.

[77] Bachman JC, Muy S, Grimaud A, Chang HH, Pour N, Lux SF, Paschos O, Maglia F, Lupart S, Lamp P, Giordano L, Shao-Horn Y. Inorganic solid-state electrolytes for lithium batteries: mechanisms and properties governing ion conduction. Chem Rev. 2016;116(1):140.

[78] Płocharski J, Wieczorek W, Przyłuski J, Such K. Mixed solid electrolytes based on poly(ethylene oxide). Appl Phys A. 1989;49(1):55.

[79] Kitajima S, Matsuda M, Yamato M, Tominaga Y. Anisotropic ionic conduction in composite polymer electrolytes filled with clays oriented by a strong magnetic field. Polym J. 2013;45(7):738.

[81] Han J, Li H, Kong D, Zhang C, Tao Y, Li H, Yang QH, Chen L. Realizing high volumetric lithium storage by compact and mechanically stable anode designs. ACS Energy Lett. 2020;5(6):1986.

[81] Shen X, Zhang R, Chen X, Cheng XB, Li XY, Zhang Q. The failure of solid electrolyte interphase on Li metal anode: structural uniformity or mechanical strength? Adv Energy Mater. 2020;10(10):8.

[82] Shen X, Zhao G, Sun K. A highly stable glass fiber host for lithium metal anode behaving enhanced coulombic efficiency. Electrochim Acta. 2019;317:333.

[83] Zheng GY, Lee SW, Liang Z, Lee HW, Yan K, Yao HB, Wang HT, Li WY, Chu S, Cui Y. Interconnected hollow carbon nanospheres for stable lithium metal anodes. Nat Nanotechnol. 2014;9(8):618.

[84] Lee H, Chen S, Ren X, Martinez A, Shutthanandan V, Vijayakumar M, Han KS, Li Q, Liu J, Xu W, Zhang JG. Electrode edge effects and the failure mechanism of lithium-metal batteries. Chemsuschem. 2018;11(21):3821.

[85] He Y, Ren XD, Xu YB, Engelhard MH, Li XL, Xiao J, Liu J, Zhang JG, Xu W, Wang CM. Origin of lithium whisker formation and growth under stress. Nat Nanotechnol. 2019;14(11):1042.

[86] Zhang X, Wang QJ, Harrison KL, Roberts SA, Harris SJ. Pressure-driven interface evolution in solid-state lithium metal batteries. Cell Rep Phys Sci. 2020;1(2):100012.

[87] Xie Y, Xiang H, Shi P, Guo J, Wang H. Enhanced separator wettability by LiTFSI and its application for lithium metal batteries. J Membr Sci. 2017;524:315.

[88] Lee H, Yanilmaz M, Toprakci O, Fu K, Zhang XW. A review of recent developments in membrane separators for rechargeable lithium-ion batteries. Energy Environ Sci. 2014;7(12):3857.

[89] Wang Z, Pan R, Xu C, Ruan C, Edström K, Strømme M, Nyholm L. Conducting polymer paper-derived separators for lithium metal batteries. Energy Storage Mater. 2018;13:283.

[90] Liang J, Chen Q, Liao X, Yao P, Zhu B, Lv G, Wang X, Chen X, Zhu J. A nano-shield design for separators to resist dendrite formation in lithium-metal batteries. Angew Chem Int Ed. 2020;59(16):6561.

[91] Xu Y, Yan H, Li T, Liu Y, Luo J, Li W, Cui X, Chen L, Yue Q, Kang Y. Can carbon sponge be used as separator in Li metal batteries? Energy Storage Mater. 2021;36:108.

[92] Monroe C, Newman J. The impact of elastic deformation on deposition kinetics at lithium/polymer interfaces. J Electrochem Soc. 2005;152:396.

[93] Ni JE, Case ED, Sakamoto JS, Rangasamy E, Wolfenstine JB. Room temperature elastic moduli and Vickers hardness of hot-pressed LLZO cubic garnet. J Mater Sci. 2012;47(23):7978.

[94] Zeng XX, Yin YX, Li NW, Du WC, Guo YG, Wan LJ. Reshaping lithium plating/stripping behavior via bifunctional polymer electrolyte for room-temperature solid Li metal batteries. J Am Chem Soc. 2016;138(49):15825.

[95] Zhou WD, Wang SF, Li YT, Xin S, Manthiram A, Goodenough JB. Plating a dendrite-free lithium anode with a polymer/ceramic/polymer sandwich electrolyte. J Am Chem Soc. 2016;138(30):9385.

[96] Xu B, Li X, Yang C, Li Y, Grundish NS, Chien PH, Dong K, Manke I, Fang R, Wu N, Xu H, Dolocan A, Goodenough JB. Interfacial chemistry enables stable cycling of all-solid-state Li metal batteries at high current densities. J Am Chem Soc. 2021;143(17):6542.

[97] Li L, Deng Y, Duan H, Qian Y, Chen G. LiF and LiNO$_3$ as synergistic additives for PEO-PVDF/LLZTO-based composite electrolyte towards high-voltage lithium batteries with dual-interfaces stability. J Energy Chem. 2022;65:319.

[98] Liu Y, Hu R, Zhang D, Liu J, Liu F, Cui J, Lin Z, Wu J, Zhu M. Constructing Li-rich artificial SEI layer in alloy-polymer composite electrolyte to achieve high ionic conductivity for all-solid-state lithium metal batteries. Adv Mater. 2021;33(11):2004711.

[99] Wang Z, Shen L, Deng S, Cui P, Yao X. 10 μm-thick high-strength solid polymer electrolytes with excellent interface compatibility for flexible all-solid-state lithium-metal batteries. Adv Mater. 2021;33(25):2100353.

[100] Lin D, Yuen PY, Liu Y, Liu W, Liu N, Dauskardt RH, Cui Y. A silica-aerogel-reinforced composite polymer electrolyte with high ionic conductivity and high modulus. Adv Mater. 2018;30(32):1802661.

[101] Fu K, Gong Y, Liu B, Zhu Y, Xu S, Yao Y, Luo W, Wang C, Lacey S, Dai J, Chen Y, Mo Y, Wachsman E, Hu L. Toward garnet electrolyte–based Li metal batteries: an ultrathin, highly effective, artificial solid-state electrolyte/metallic Li interface. Sci Adv. 2017;3:1601659.

[102] Li X, Liu J, Banis MN, Lushington A, Li R, Cai M, Sun X. Atomic layer deposition of solid-state electrolyte coated cathode materials with superior high-voltage cycling behavior for lithium ion battery application. Energy Environ Sci. 2014;7(2):768.

[103] Duan J, Huang L, Wang T, Huang Y, Fu H, Wu W, Luo W, Huang Y. Shaping the contact between Li metal anode and solid-state electrolytes. Adv Funct Mater. 2020;30(15):1908701.

[104] Duan J, Wu W, Nolan AM, Wang T, Wen J, Hu C, Mo Y, Luo W, Huang Y. Lithium–graphite paste: an interface compatible

anode for solid-state batteries. Adv Mater. 2019;31(10): 1807243.

[105] Huang Y, Chen B, Duan J, Yang F, Wang T, Wang Z, Yang W, Hu C, Luo W, Huang Y. Graphitic carbon nitride (g-C$_3$N$_4$): an interface enabler for solid-state lithium metal batteries. Angew Chem Int Ed. 2020;59(9):3699.

[106] Parekh MN, Rahn CD, Archer LA. Controlling dendrite growth in lithium metal batteries through forced advection. J Power Sour. 2020;452:227760.

[107] Shen L, Shi P, Hao X, Zhao Q, Ma J, He YB, Kang F. Progress on lithium dendrite suppression strategies from the interior to exterior by hierarchical structure designs. Small. 2020;16(26): 2000699.

[108] Zuo TT, Wu XW, Yang CP, Yin YX, Ye H, Li NW, Guo YG. Graphitized carbon fibers as multifunctional 3D current collectors for high areal capacity Li anodes. Adv Mater. 2017; 29(29):1700389.

[109] Tang Y, Sha JW, Wang N, Zhang R, Ma LY, Shi CS, Liu EZ, Zhao NQ. Covalently bonded 3D rebar graphene foam for ultrahigh-areal-capacity lithium-metal anodes by in-situ loose powder metallurgy synthesis. Carbon. 2020;158:536.

[110] Wang Y, Wang Z, Lei D, Lv W, Zhao Q, Ni B, Liu Y, Li B, Kang F, He YB. Spherical Li deposited inside 3D Cu skeleton as anode with ultrastable performance. ACS Appl Mater Interfaces. 2018;10(24):20244.

[111] Ryou MH, Yong ML, Lee Y, Winter M, Bieker P. Mechanical surface modification of lithium metal: towards improved Li metal anode performance by directed Li plating. Adv Funct Mater. 2015;25(6):834.

[112] Lu LL, Ge J, Yang JN, Chen SM, Yao H, Zhou F, Yu SH. Free-standing copper nanowire network current collector for improving lithium anode performance. Nano Lett. 2016;16: 4431.

[113] Fang Y, Zeng Y, Jin Q, Lu XF, Luan D, Zhang X, Lou XW. Nitrogen-doped amorphous Zn-carbon multichannel fibers for stable lithium metal anodes. Angew Chem Int Ed. 2021;60(15): 8515.

[114] Wang CY, Zheng ZJ, Feng YQ, Ye H, Cao FF, Guo ZP. Topological design of ultrastrong MXene paper hosted Li enables ultrathin and fully flexible lithium metal batteries. Nano Energy. 2020;74:104817.

[115] Xue P, Liu S, Shi X, Sun C, Lai C, Zhou Y, Sui D, Chen Y, Liang J. A hierarchical silver-nanowire–graphene host enabling ultrahigh rates and superior long-term cycling of lithium-metal composite anodes. Adv Mater. 2018;30(44): 1804165.

[116] Wang X, Pawar G, Li Y, Ren X, Zhang M, Lu B, Banerjee A, Liu P, Dufek EJ, Zhang JG, Xiao J, Liu J, Meng YS, Liaw B. Glassy Li metal anode for high-performance rechargeable Li batteries. Nat Mater. 2020;19(12):1339.

[117] Mahmood N, Zhu J, Rehman S, Li Q, Hou Y. Control over large-volume changes of lithium battery anodes via active–inactive metal alloy embedded in porous carbon. Nano Energy. 2015;15:755.

[118] Guo F, Wang Y, Kang T, Liu C, Shen Y, Lu W, Wu X, Chen L. A Li-dual carbon composite as stable anode material for Li batteries. Energy Storage Mater. 2018;15:116.

[119] Liu S, Zhang X, Li R, Gao L, Luo J. Dendrite-free Li metal anode by lowering deposition interface energy with Cu$_{99}$Zn alloy coating. Energy Storage Mater. 2018;14:143.

[120] Wang ZY, Lu ZX, Guo W, Luo Q, Yin YH, Liu XB, Li YS, Xia BY, Wu ZP. A dendrite-free lithium/carbon nanotube hybrid for lithium-metal batteries. Adv Mater. 2020;33(4): 2006702.

[121] Zhou Y, Zhang X, Ding Y, Zhang L, Yu G. Reversible deposition of lithium particles enabled by ultraconformal and stretchable graphene film for lithium metal batteries. Adv Mater. 2020;32(48):2005763.

[122] Cheng XB, Hou TZ, Zhang R, Peng HJ, Zhao CZ, Huang JQ, Zhang Q. Dendrite-free lithium deposition induced by uniformly distributed lithium ions for efficient lithium metal batteries. Adv Mater. 2016;28(15):2888.

[123] Wang H, Hu P, Liu X, Shen Y, Yuan L, Li Z, Huang Y. Sowing silver seeds within patterned ditches for dendrite-free lithium metal batteries. Adv Sci. 2021;8(14):2100684.

[124] Yang G, Liu Z, Weng S, Zhang Q, Wang X, Wang Z, Gu L, Chen L. Iron carbide allured lithium metal storage in carbon nanotube cavities. Energy Storage Mater. 2021;36:459.

[125] Wang J, Yi S, Liu J, Sun S, Liu Y, Yang D, Xi K, Gao G, Abdelkader A, Yan W, Ding S, Kumar RV. Suppressing the shuttle effect and dendrite growth in lithium–sulfur batteries. ACS Nano. 2020;14(8):9819.

[126] Zou P, Wang Y, Chiang SW, Wang X, Kang F, Yang C. Directing lateral growth of lithium dendrites in micro-compartmented anode arrays for safe lithium metal batteries. Nat Commun. 2018;9(1):464.

[127] Wang AX, Zhang XY, Yang YW, Huang JX, Liu XJ, Luo JY. Horizontal centripetal plating in the patterned voids of Li/graphene composites for stable lithium-metal anodes. Chem. 2018;4(9):2192.

[128] Tao Y, Sui ZY, Han BH. Advanced porous graphene materials: from in-plane pore generation to energy storage applications. J Mater Chem A. 2020;8(13):6125.

[129] Antink WH, Choi Y, Seong KD, Kim JM, Piao Y. Recent progress in porous graphene and reduced graphene oxide-based nanomaterials for electrochemical energy storage devices. Adv Mater Interfaces. 2018;5(5):1701212.

[130] Wang P, Zhang G, Wei XY, Liu R, Gu JJ, Cao FF. Bioselective synthesis of a porous carbon collector for high-performance sodium-metal anodes. J Am Chem Soc. 2021;143(9):3280.

[131] Lu Y, Lu Y, Jin C, Gao R, Liu B, Huang Y, Yu Y, Ren J, Deng Y, Tao X, Lyu J. Natural wood structure inspires practical lithium–metal batteries. ACS Energy Lett. 2021;6(6):2103.

[132] Zhang R, Chen X, Shen X, Zhang XQ, Chen XR, Cheng XB, Yan C, Zhao CZ, Zhang Q. Coralloid carbon fiber-based composite lithium anode for robust lithium metal batteries. Joule. 2018;2(4):764.

[133] Meng JK, Wang WW, Yue XY, Xia HY, Wang QC, Wang XX, Fu ZW, Wu XJ, Zhou YN. Cotton-derived carbon cloth enabling dendrite-free Li deposition for lithium metal batteries. J Power Sour. 2020;465:228291.

[134] Jin C, Sheng O, Luo J, Yuan H, Fang C, Zhang W, Huang H, Gan Y, Xia Y, Liang C, Zhang J, Tao X. 3D lithium metal embedded within lithiophilic porous matrix for stable lithium metal batteries. Nano Energy. 2017;37:177.

[135] Zhang S, Zheng M, Lin Z, Li N, Liu Y, Zhao B, Pang H, Cao J, He P, Shi Y. Activated carbon with ultrahigh specific surface area synthesized from natural plant material for lithium–sulfur batteries. J Mater Chem A. 2014;2(38):15889.

[136] Yang T, Sun Y, Qian T, Liu J, Liu X, Rosei F, Yan C. Lithium dendrite inhibition via 3D porous lithium metal anode accompanied by inherent SEI layer. Energy Storage Mater. 2020;26:385.

[137] Xu Q, Yang X, Rao M, Lin D, Yan K, Du R, Xu J, Zhang Y, Ye D, Yang S, Zhou G, Lu Y, Qiu Y. High energy density lithium metal batteries enabled by a porous graphene/MgF$_2$ framework. Energy Storage Mater. 2020;26:73.

[138] Wei C, Tan L, Tao Y, An Y, Tian Y, Jiang H, Feng J, Qian Y. Interfacial passivation by room-temperature liquid metal enabling stable 5 V-class lithium-metal batteries in commercial carbonate-based electrolyte. Energy Storage Mater. 2021;34: 12.

[139] Lin L, Suo L, Hu YS, Li H, Huang X, Chen L. Epitaxial induced plating current-collector lasting lifespan of anode-free lithium metal battery. Adv Energy Mater. 2021;11(9):2003709.

[140] Zhang S, Deng W, Zhou X, He B, Liang J, Zhao F, Guo Q, Liu Z. Controlled lithium plating in three-dimensional hosts through nucleation overpotential regulation toward high-areal-capacity lithium metal anode. Mater Today Energy. 2021;21:100770.

[141] Li J, Zou P, Chiang SW, Yao W, Wang Y, Liu P, Liang C, Kang F, Yang C. A conductive-dielectric gradient framework for stable lithium metal anode. Energy Storage Mater. 2020;24:700.

[142] Hong SH, Jung DH, Kim JH, Lee YH, Cho SJ, Joo SH, Lee HW, Lee KS, Lee SY. Electrical conductivity gradient based on heterofibrous scaffolds for stable lithium-metal batteries. Adv Funct Mater. 2020;30(14):1908868.

[143] Yun J, Park BK, Won ES, Choi SH, Kang HC, Kim JH, Park MS, Lee JW. Bottom-up lithium growth triggered by interfacial activity gradient on porous framework for lithium-metal anode. ACS Energy Lett. 2020;5(10):3108.

[144] Zhai P, Wang T, Jiang H, Wan J, Wei Y, Wang L, Liu W, Chen Q, Yang W, Cui Y, Gong Y. 3D artificial solid-electrolyte interphase for lithium metal anodes enabled by insulator–metal–insulator layered heterostructures. Adv Mater. 2021;33(13):2006247.

[145] Li QH, Xu C, Huang B, Yin X. Sr^{2+}-doped rhombohedral $LiHf_2(PO_4)_3$ solid electrolyte for all-solid-state Li-metal battery. Rare Met. 2020;39(9):1092.

[146] Xu S, McOwen DW, Zhang L, Hitz GT, Wang C, Ma Z, Chen C, Luo W, Dai J, Kuang Y, Hitz EM, Fu K, Gong Y, Wachsman ED, Hu L. All-in-one lithium-sulfur battery enabled by a porous-dense-porous garnet architecture. Energy Storage Mater. 2018;15:458.

[147] Yun Q, He YB, Lv W, Zhao Y, Li B, Kang F, Yang QH. Chemical dealloying derived 3D porous current collector for Li metal anodes. Adv Mater. 2016;28(32):6932.

[148] Zhang R, Cheng XB, Zhao CZ, Peng HJ, Shi J, Huang JQ, Wang J, Wei F, Zhang Q. Conductive nanostructured scaffolds render low local current density to inhibit lithium dendrite growth. Adv Mater. 2016;28(11):2155.

[149] Zhu W, Deng W, Zhao F, Liang S, Zhou X, Liu Z. Graphene network nested Cu foam for reducing size of lithium metal towards stable metallic lithium anode. Energy Storage Mater. 2019;21:107.

[150] Liu L, Yin YX, Li JY, Li NW, Zeng XX, Ye H, Guo YG, Wan LJ. Free-standing hollow carbon fibers as high-capacity containers for stable lithium metal anodes. Joule. 2017;1(3):563.

[151] Chi SS, Wang Q, Han B, Luo C, Jiang Y, Wang J, Wang C, Yu Y, Deng Y. Lithiophilic Zn sites in porous CuZn alloy induced uniform Li nucleation and dendrite-free Li metal deposition. Nano Lett. 2020;20(4):2724.

[152] Fang Y, Zeng Y, Jin Q, Lu XF, Luan D, Zhang X, Lou XW. Nitrogen-doped amorphous Zn-carbon multichannel fibers for stable lithium metal anodes. Angew Chem Int Ed. 2021;60(15):8515.

[153] Li S, Zhang S, Sun C, Zhao W, Zhao T, Zhang M, Wang H, Ma Y. Honeycomb inspired lithiophilic scaffold for ultra-stable, high-areal-capacity metallic deposition. Energy Storage Mater. 2021;35:378.

[154] Chen H, Yang Y, Boyle DT, Jeong YK, Xu D, Vasconcelos LS, Huang Z, Wang H, Wang H, Huang W, Li H, Wang J, Gu H, Matsumoto R, Motohashi K, Nakayama Y, Zhao K, Cui Y. Free-standing ultrathin lithium metal-graphene oxide host foils with controllable thickness for lithium batteries. Nat Energy. 2021;6(8):790.

[155] Chen C, Guan J, Li NW, Lu Y, Luan D, Zhang CH, Cheng G, Yu L, Lou XW. Lotus-root-like carbon fibers embedded with Ni–Co nanoparticles for dendrite-free lithium metal anodes. Adv Mater. 2021;33(24):2100608.

[156] Tao L, Xu Z, Kuai C, Zheng X, Wall CE, Jiang C, Esker AR, Zheng Z, Lin F. Flexible lignin carbon membranes with surface ozonolysis to host lean lithium metal anodes for nickel-rich layered oxide batteries. Energy Storage Mater. 2020;24:129.

[157] Qin K, Baucom J, Liu DL, Shi WY, Zhao NQ, Lu YF. A powder metallurgic approach toward high-performance lithium metal anodes. Small. 2020;16(24):2000794.
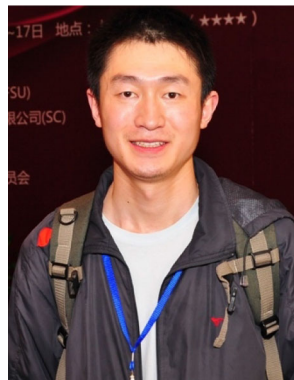
Yao Li received his Ph.D. degree in Material Science and Engineering from Shanghai Jiao Tong University, China, in 2015. He joined as a research associate at State Key Laboratory of Metal Matrix Composites, School of Materials Science and Engineering, Shanghai Jiao Tong University in 2015. He has been a visiting scholar in Massachusetts Institute of Technology during Dec. 2019 and Apr. 2021. His current research includes bioinspired material and carbon matrix material, as well as their application on environment treatment and energy storage.

Sa Li completed her Ph.D. degree with Prof. Chang-An Wang in Materials Science and Engineering from Tsinghua University, China, in 2015. Afterward, she joined the School of Materials Science and Engineering at Tongji University as an assistant professor until now. Her current research interest is mainly on designing advanced anode materials for lithium-ion batteries and Li–S batteries.